

**The Determination of Cloud Optical Depth from Multiple Fields of  
View Pyrheliometric Measurements**

by  
Robert Alan Raschke and Stephen K. Cox

Department of Atmospheric Science  
Colorado State University  
Fort Collins, Colorado



**Department of  
Atmospheric Science**

Paper No. 361

THE DETERMINATION OF CLOUD OPTICAL DEPTH FROM MULTIPLE FIELDS OF VIEW  
PYRHELIOMETRIC MEASUREMENTS

By

Robert Alan Raschke

and

Stephen K. Cox

Research supported by  
The National Science Foundation  
Grant No. ATM-8010691

Department of Atmospheric Science  
Colorado State University  
Fort Collins, Colorado

December, 1982

Atmospheric Science Paper Number #361

## ABSTRACT

The feasibility of using a photodiode radiometer to infer optical depth of thin clouds from solar intensity measurements was examined. Data were collected from a photodiode radiometer which measures incident radiation at angular fields of view of  $2^\circ$ ,  $5^\circ$ ,  $10^\circ$ ,  $20^\circ$ , and  $28^\circ$ . In combination with a pyrliometer and pyranometer, values of normalized annular radiance and transmittance were calculated. Similar calculations were made with the results of a Monte Carlo radiative transfer model. The Monte Carlo results were for cloud optical depths of 1 through 6 over a spectral bandpass of 0.3 to  $2.8 \mu\text{m}$ .

Eight case studies involving various types of high, middle, and low clouds were examined. Experimental values of cloud optical depth were determined by three methods. Plots of transmittance versus field of view were compared with the model curves for the six optical depths which were run in order to obtain a value of cloud optical depth. Optical depth was then determined mathematically from a single equation which used the five field of view transmittances and as the average of the five optical depths calculated at each field of view. Analysis of the case study results indicates that the photodiode radiometer can be used effectively to determine the optical depth of thin clouds.

#### ACKNOWLEDGEMENTS

The authors wish to express their appreciation to Professors Richard H. Johnson and Dale Winder for their thoughtful review of this research. We also greatly appreciate the help of Dr. John M. Davis during our many consultations on the use of the Monte Carlo radiative transfer model. Special thanks are due to Chris Pasqua and Charles Wilkins for their work with the instrumentation, to John Graffy for his expert programming advice, To Duayne Barnhart for his photographic work, to Ms. Judy Sorbie for drafting the figures and to Ms. Melissa Tucker for typing the many drafts of this paper as well as the final manuscript.

This research was supported by National Science Foundation Grant No. ATM-8010691.

## TABLE OF CONTENTS

	<u>Page</u>
1.0 Introduction	1
2.0 Instrumentation	9
2.1 Description	9
2.2 Calibration	14
3.0 Radiative Transfer Model	17
3.1 Description	17
3.2 Model Results	22
4.0 Data Reduction Procedures	26
5.0 Comparison of Model and Experimental Results	29
5.1 Procedures	29
5.2 Case Studies	34
5.21 High Clouds	34
5.22 Mid-level Clouds	52
5.23 Low-level Clouds	58
5.3 Discussion	73
6.0 Conclusion	81
References	85

LIST OF TABLES

<u>Table</u>	<u>Page</u>
1 Dimensions of the collimator tubes.	11
2 Physical dimensions of the PV-100A photodiodes.	14
3 Sensitivities of the photodiodes for the clear case, the diffuse case, and the average sensitivity.	16
4 Input parameters used in the Monte Carlo model.	19
5 Energy values of incident, reflected, absorbed, and transmitted radiation for cloud optical depths of 1 to 6 obtained from the Monte Carlo model. All energy values are in $W/M^2$ .	24
6 Normalized radiance values calculated for cloud optical depths of 1 to 6.	24
7 Transmittance values calculated for cloud optical depths of 1 to 6.	25
8 Summary of sky conditions on data collection days. The precipitable water values are those given for Denver, Colorado, and were taken from NMC facsimile charts. NA indicates not available.	26
9 Values of coefficients in Equation 19.	30
10 Calculated versus expected values of $\tau$ using model transmittances and Equation 19.	30
11 Coefficients of the curves relating transmittance to optical depth for the five fields of view. The equations have the form $y = a + blnx$ .	33
12 Calculated optical depths for the period 1055-1104 MST October 28th, 1981.	39
13 Calculated optical depths for the period 1216-1225 MST October 26th, 1981.	44
14 Calculated optical depths for the period 1036-1045 MST November 13, 1981.	46

15	Calculated optical depths for the period 1216-1225 MST February 22, 1982.	53
16	Calculated optical depths for the period 1021-1030 MST November 23, 1981.	55
17	Calculated optical depths for the period 1016-1025 MST January 12, 1982.	62
18	Calculated optical depths for the period 1326-1335 MST January 12, 1982.	67
19	Calculated optical depths for the period 1426-1435 MST April 15, 1982.	72
20	Results of the sensitivity test on the two methods of calculating cloud optical depth.	78

LIST OF FIGURES

<u>Figure</u>	<u>Page</u>
1 Transmittance versus field of view for Monte Carlo cloud optical depths of 1, 3, and 6.	6
2 Transmittance versus optical depth for a 28° field of view as produced by the Monte Carlo model.	8
3 Instrumentation used for the determination of cloud optical depth.	10
4 Close-up of the photodiode radiometer.	10
5 Design of the photodiode - collimator tube combination.	12
6 Relative spectral response of the PV-100A photodiodes.	13
7 Current to voltage amplifier design including the pin configuration for a MC 47416 chip.	15
8 Single scattering phase functions for the two spectral bandpasses used in the MC model.	20
9 Cumulative probability distribution for both spectral bandpasses used in the MC model.	21
10 Optical depth versus transmittance for 2°, 5°, 10°, 20°, and 28° fields of view produced from the Monte Carlo model.	32
11a Photograph of cloud cover at 1100 MST October 28, 1981.	35
11b Photograph of cloud cover at 1220 MST October 26, 1981.	35
11c Photograph of cloud cover at 1040 MST November 13, 1981.	36
12a Transmittance versus field of view for 1100 MST October 28, 1981.	37
12b Ten minute average values of transmittance versus field of view for the period 1055-1104 MST October 28, 1981.	38

12c	Transmittance versus field of view for 1220 MST October 26, 1981.	42
12d	Ten minute average values of transmittance versus field of view for the period 1216-1225 MST October 26, 1981.	43
12e	Transmittance versus field of view for 1040 MST November 13, 1981.	47
12f	Ten minute average values of transmittance versus field of view for the period 1036-1045 MST November 13, 1981.	48
12g	Transmittance versus field of view for 1221 MST February 22, 1982.	50
12h	Ten minute average values of transmittance versus field of view for the period 1216-1225 MST February 22, 1982.	51
13	Photograph of cloud cover at 1030 MST November 23, 1981.	54
14a	Transmittance versus field of view for 1025 MST November 23, 1981.	56
14b	Ten minute average values of transmittance versus field of view for the period 1021-1030 MST November 23, 1981.	57
15a	Transmittance versus field of view for 1020 MST January 12, 1982.	60
15b	Ten minute average values of transmittance versus field of view for the period 1016-1025 MST January 12, 1982.	61
15c	Transmittance versus field of view for 1330 MST January 12, 1982.	64
15d	Ten minute average values of transmittance versus field of view for the period 1326-1335 MST January 12, 1982.	65
15e	Transmittance versus field of view for 1430 MST April 15, 1982.	68
15f	Ten minute average values of transmittance versus field of view for the period 1426-1435 MST April 15, 1982.	70
16	Photograph of cloud cover at 1425 MST April 15, 1982.	71
17	Total intensity, $i$ , for randomly oriented herogonal prisms compared with that for spheres versus scattering angle $\theta$ .	75
18	The angular scattering function for Mie scattering as a function of the cosine of the scattering angle $\theta$ for six particle size distributions.	76

## 1.0 INTRODUCTION

The potential impact of clouds on the earth's radiation budget and subsequently upon the climate has been acknowledged for over a century. However, a clear understanding of the magnitude of the effect and even whether clouds represent a positive or a negative feedback upon climate, still eludes us. Much of the lack of understanding comes from a lack of knowledge of the radiative properties of clouds. The magnitude and the sign of the effect of clouds upon terrestrial climate depends upon not only cloud cover and cloud height, but also upon the average solar reflectance and transmittance of the clouds and the clouds' infrared emittance. This effect is clearly shown in the work of Manabe and Strickler (1964), Cox (1971), and Bowling (1972).

Several authors have discussed the possible effects of clouds on climate. Cess (1976) examined the effect that a change in cloud amount would have on climate. He concludes that cloud amount is an insignificant feedback mechanism affecting climate both zonally and globally because the effects of changes in infrared opacity are exactly compensated by the effects caused by changes in cloud albedo. Cess and Ramanathan (1978) suggest that as cloud amount increases, the fraction of high clouds increases and the fraction of low clouds decreases thus increasing the greenhouse effect. This was cited as the reason why the amount of LW radiation lost to space was found to be much less for satellite observations than the amount predicted from

model calculations. Using this fact, Cess and Ramanathan also concluded that the effect on climate caused by a change in cloud amount is negligible because the greenhouse effect cancels the albedo effect. Ellis (1978), on the other hand, concludes that clouds are significant climate feedback mechanisms. His work suggests that an increase in cloud amount will cause a decrease in surface temperature if all other factors are held constant. Ohring and Clapp (1980) found that the net radiation at the top of the atmosphere is sensitive to cloud amount changes and the sensitivity is such that the albedo effect dominates the greenhouse effect.

If the conclusion by Ohring, Clapp and Ellis that clouds are an important climate feedback mechanism is correct, then the need exists to determine the various radiative and physical properties of clouds and apply them in climate models. One such parameter is cloud optical depth. Ohring and Adler (1978) used a zonally averaged climate model in which a single cloud layer is assumed at each latitude belt. A specified cloud amount, altitude, and optical depth were given for the cloud layer. Since the albedo of the cloud depends on the cloud optical depth, the concept of optical depth is very important in this model. Ohring and Adler assigned optical depths of 2, 8, and 16 to high, middle, and low clouds respectively. Optical depths for various latitude bands were calculated by weighting the amount of high, middle, and low clouds in the particular latitude bands. The cloud optical depth was adjusted to a value of 7 in order to produce similar observed and computed average hemispheric planetary albedo and surface temperatures. In this climate model, the optical depth was specified for different cloud heights. It would be beneficial, then, to be able

to make actual measurements of cloud optical depths and apply them in the various climate models.

The primary objective of this paper is to determine the feasibility of using a photodiode radiometer to classify thin clouds according to their optical depth. The method used employs a relationship between the bulk scattering properties of a cloud and its optical depth. As the optical thickness of the cloud increases, one expects more scattering of incident radiation and consequently a depletion of the direct beam. This scattering has been effectively reproduced through the use of Monte Carlo cloud models. However, very little actual data has been collected which shows the extent of the scattering for different cloud types. Thompson and Cox (1982) used data from a normal incidence pyrheliometer to measure the changing transmittance of the direct solar beam. Transmittance values determined from the pyrheliometer outputs were classified into one of three categories, clear, thin cloud, or thick cloud, based on the magnitude of the transmittance values obtained. An instrument has been developed which relies on the same principle. This instrument uses five silicon photodiode detectors, each with a different angular field of view, to measure the energy scattered at small angles from the direct beam. The data collected are compared with the results of the Monte Carlo radiative transfer model.

Coulson (1975) presents the classical definition for the optical depth above a height  $z$  as:

$$\tau(\lambda, z) = \int_z^{\infty} B(\lambda, z) dz \quad (1)$$

where  $B$  is the attenuation coefficient. The value of  $\tau(\lambda, z)$  is an

indicator of the energy lost by a beam of radiation of a given wavelength  $\lambda$  after it has travelled a distance  $z$ . By analogy, the broadband optical depth is simply:

$$\tau = \int_z^{\infty} B dz \quad (2)$$

This total optical depth  $\tau$  may be defined further as:

$$\tau = \tau_s + \tau_a \quad (3)$$

where  $\tau_s$  is the scattering optical depth and  $\tau_a$  is the absorption optical depth.

Cloud optical depth has been used in several other radiation studies. Twomey (1976) defined total optical depth as:

$$\tau = \tau_s + \tau_a + \tau_v \quad (4)$$

where  $\tau_s$  is the scattering optical thickness for 1 Km layer,  $\tau_a$  is the absorption optical thickness for drops, and  $\tau_v$  is the absorption optical thickness for a 1 Km path of water vapor. The values of  $\tau$  were found from the relationship

$$\tau = 2^n \tau_o \quad (5)$$

where  $\tau_o = 2^{-10}$  and were used in a study of the absorption of solar radiation by clouds. Stephens (1978) defined cloud optical thickness as:

$$\tau_{n\lambda} = \int_0^{\Delta z} \int_0^{\infty} n(r) Q_{EXT}(x) \pi r^2 dr dz \quad (6)$$

where  $x = 2\pi r/\lambda$ ,  $n(r)$  is the cloud droplet size distribution,  $r$  is the droplet radius, and  $Q_{EXT}(x)$  is the efficiency factor for extinction

which is determined from Mie theory. Since  $Q_{EXT}(x)$  varies only slightly with the size parameter  $x$  especially for large  $x$ , Eq. 6 reduces to the form:

$$\tau_n = \int_0^{\Delta z} 2\pi \left[ \int_0^\infty n(r)r^2 dr \right] dz \quad (7)$$

at shorter wavelengths. If the effective radius is defined as:

$$r_e = \int_0^\infty n(r)r^3 dr / \int_0^\infty n(r)r^2 dr \quad (8)$$

the Eq. 7 becomes:

$$\tau_n \approx \frac{3}{2} \frac{W}{r_e} \quad (9)$$

where  $W$  is the liquid water path and  $r_e$  is the effective droplet radius. The values of optical depth were used in a scheme to determine the shortwave absorption, albedo, and longwave emissivity of water clouds.

To determine the effectiveness of the photodiode radiometer in measuring cloud optical depth, values of normalized annular radiance and transmittance are calculated from data collected from various cloud types. These values are compared graphically and mathematically with similar computations made using the results from the Monte Carlo radiative transfer model. Model results were obtained for cloud optical depths of 1 through 6. The graphical comparison will be made using plots of transmittance versus field of view as shown in Figure 1. This figure shows the curves of transmittance for cloud optical depths of 1, 3, and 6. Equations are also derived to calculate an experimental optical depth using both the transmittance and normalized radiance values.

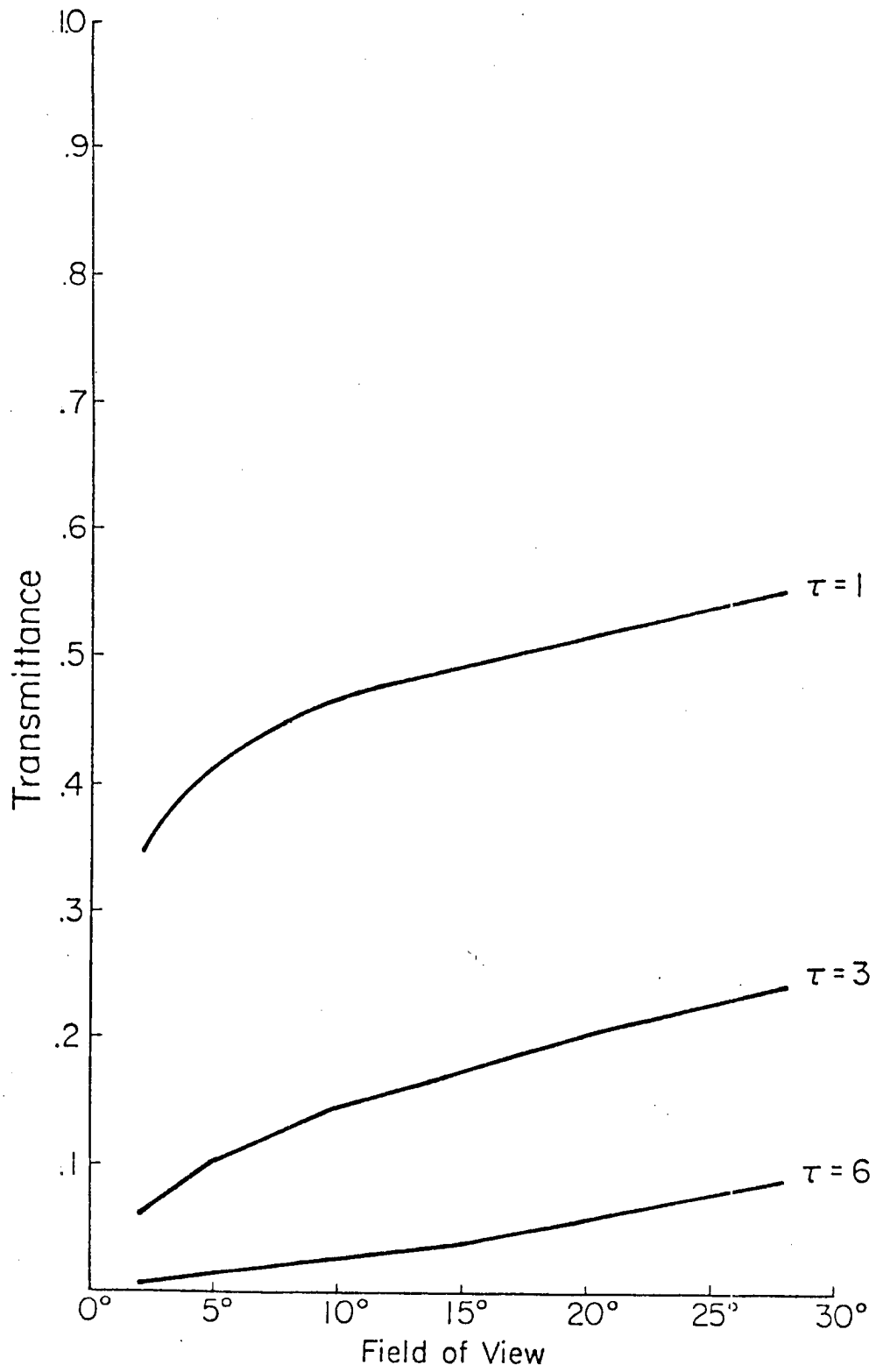


Figure 1. Transmittance versus field of view for Monte Carlo model cloud optical depths of 1, 3, and 6.

The Monte Carlo model was run for cloud optical depths less than 10 because it was felt that the largest variability in transmittances would be obtained at small optical depths. The value of transmittance should not be significantly different for optical depths of 10 and 100 especially at small fields of view. The plot of transmittance versus optical depth in Figure 2 confirms the fact that for the largest photodiode field of view, the greatest variability in the transmittance occurs at optical depths less than 6. The solid portion of the curve is obtained directly from model results while the dashed portion is obtained by using the equation of the model curve to calculate the optical depths for smaller values of transmittance.

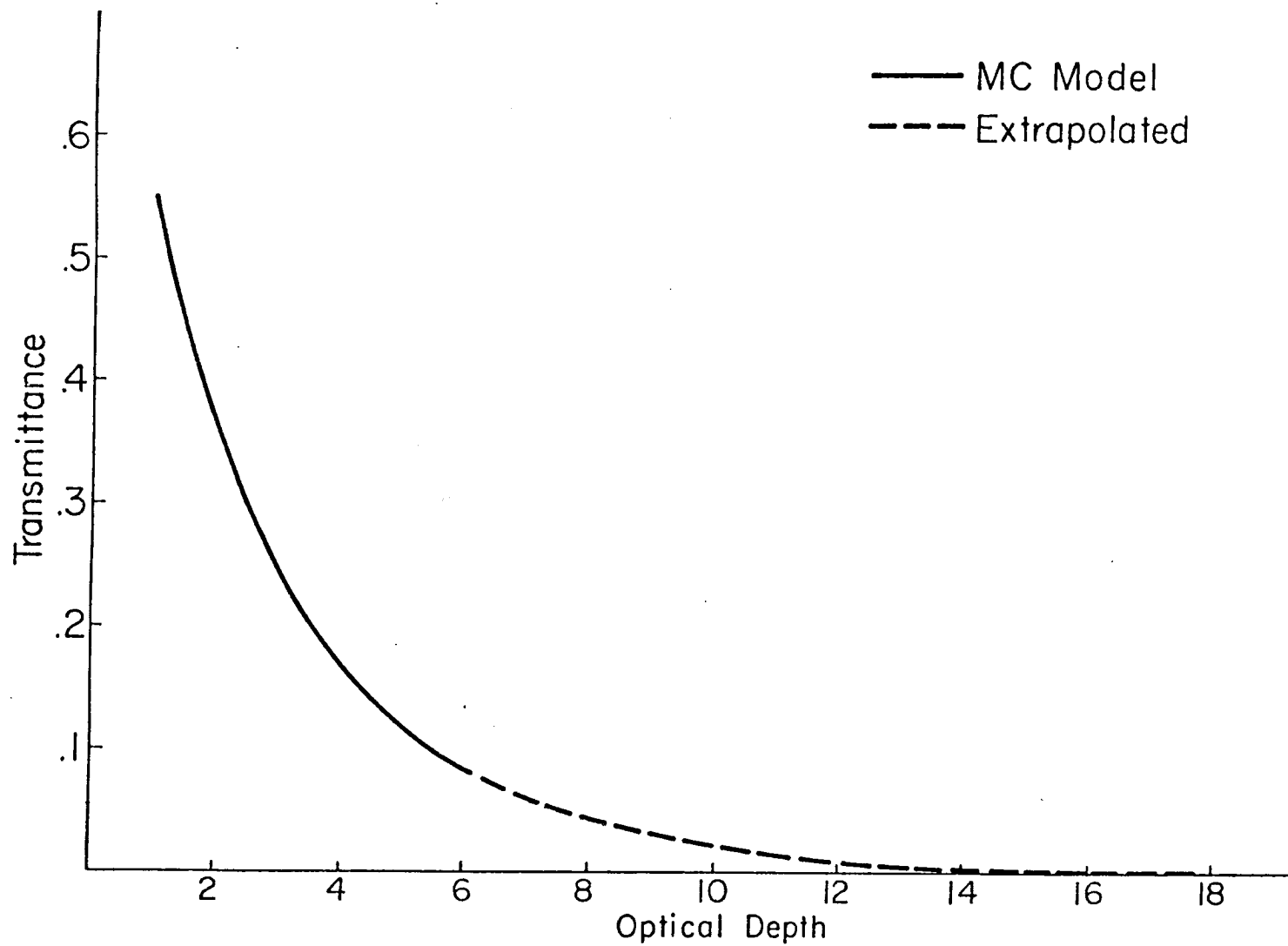


Figure 2. Transmittance versus optical depth for a 28° field of view as produced by the Monte Carlo model.

## 2.0 INSTRUMENTATION

### 2.1 Description

Data were collected from three instruments which were mounted on an equatorial tracking system and located on the roof of the Atmospheric Science facility at Colorado State University. The instruments and the tracking device are shown in Figure 3. An Eppley pyrhelimeter was used to measure the direct component of the incident solar radiation. The pyrhelimeter has an aperture design which limits its full angle field of view to 5.7 degrees. An Eppley pyranometer was used to measure the total radiation in a plane perpendicular to the direct solar beam. Technical characteristics of the pyranometer and pyrhelimeter are listed below:

	<u>Pyrhelimeter</u>	<u>Pyranometer</u>
1) Range in which radiation is measured	.285 - 2.8 $\mu\text{m}$	.285 - 2.8 $\mu\text{m}$
2) Peak sensitivity	.00739 MV/W-M <sup>-2</sup>	.00857 MV/W-M <sup>-2</sup>

The third radiometer, especially designed for this program, is really five instruments. This device employed five silicon photodiodes each collimated to achieve a different full angle field of view. A photograph of this instrument is shown in Figure 4. Table 1 lists the fields of view of the five photodiodes and the dimensions of the collimator tubes used to achieve these fields of view. Figure 5 shows the design of the collimator tube-photodiode combination.



Figure 3. Instrumentation used for the determination of cloud optical depth.

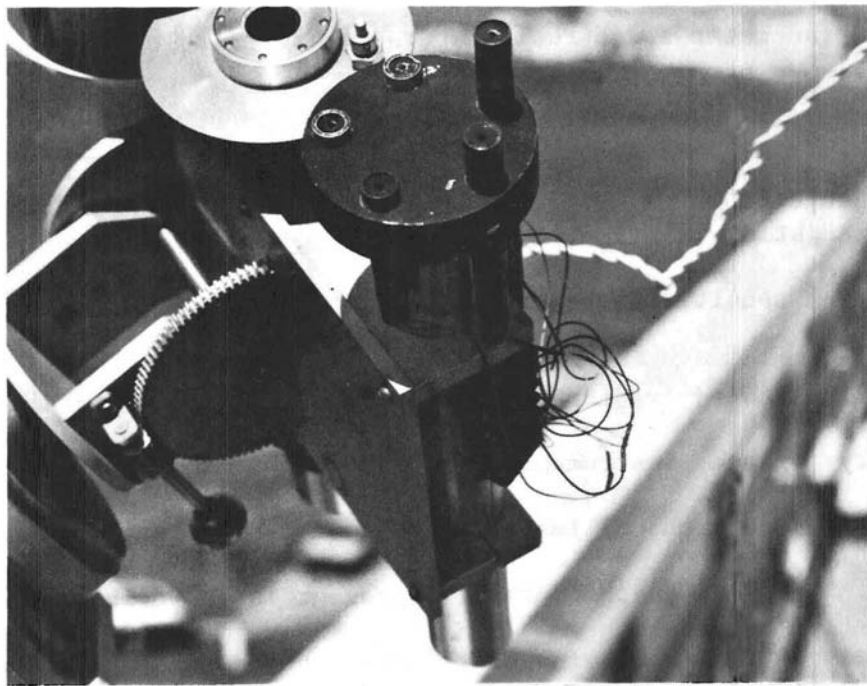


Figure 4. Close-up of the photodiode radiometer.

Table 1. Dimensions of the collimator tubes. All dimensions are in millimeters.

<u>Field of View</u>	<u>Length</u>	<u>Aperture Size</u>
1.99°	144.8	2.5
5.05°	57.2	2.5
9.87°	29.2	2.5
20.54°	14.0	2.5
28.04°	10.2	2.5

As shown in Figure 5, the collimator tubes are constructed with an aperture at each end separated by a hollow spacer. The aperture size is constant for each collimator with the spacer length varied to achieve the desired field of view. This design was chosen to reduce scattering inside the collimator tube and to make calibration easier. The interior surfaces of the collimators are painted with a flat black paint to reduce scattering inside the tube.

The silicon photodiodes used are series PV-100A manufactured by EG&G Ortec's Electro-Optics division. These diodes have a spectral bandpass from 0.35 microns to 1.15 microns. The relative spectral response of the diodes is shown in Figure 6. Table 2 lists the physical dimensions of photodiodes.

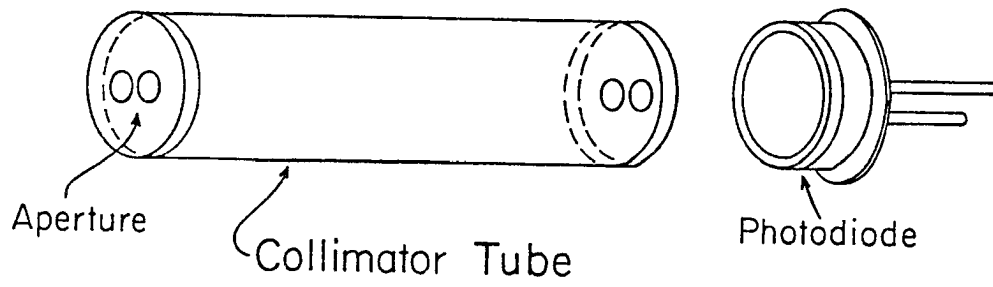


Figure 5. Design of the photodiode-collimator tube combination.

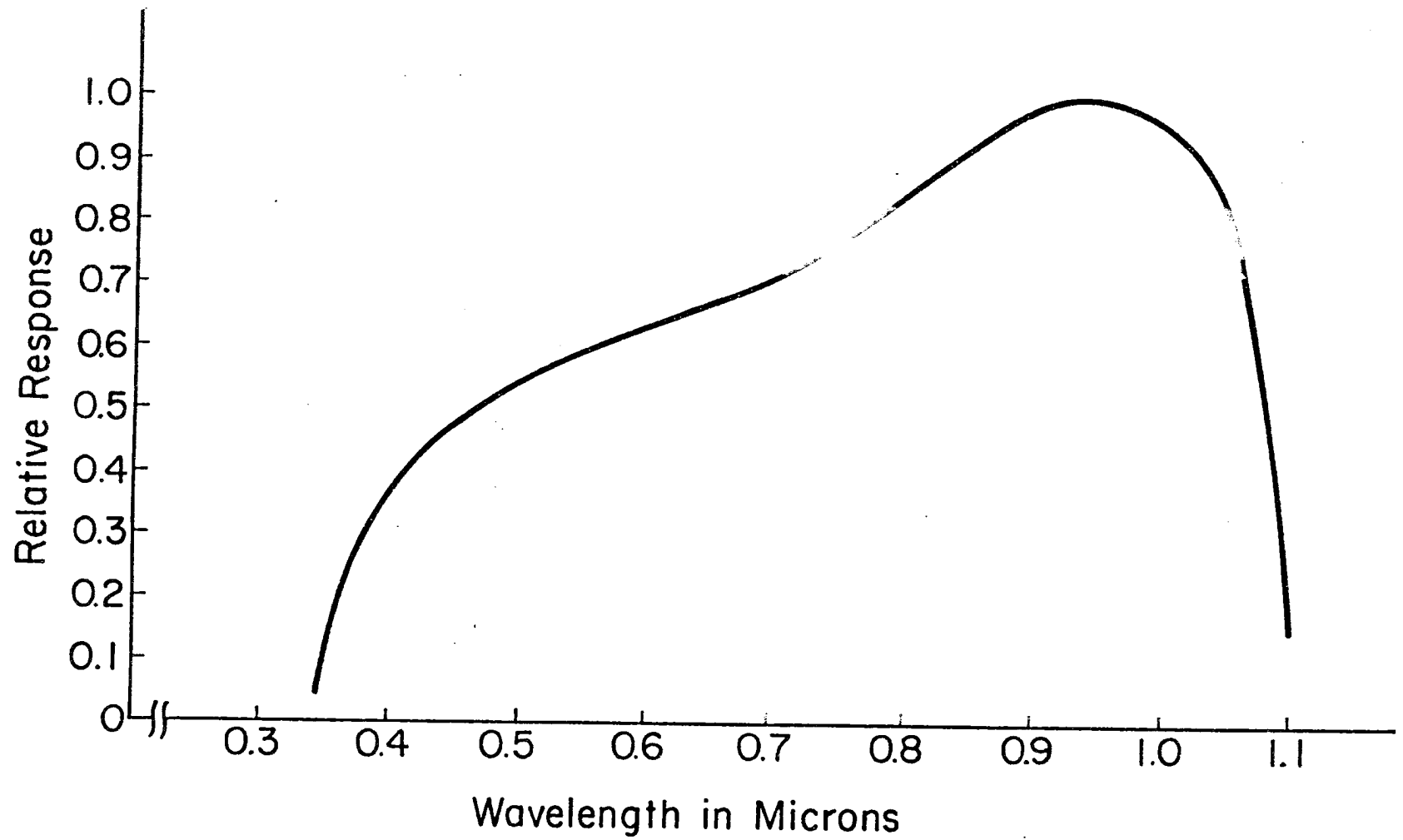


Figure 6. Relative spectral response of the PV-100A photodiodes.

Table 2. Physical dimensions of the PV-100A photodiodes.

<u>Characteristic</u>	<u>Dimension</u>
Active Area	5.1 MM <sup>2</sup>
Window Thickness	1.3 MM
Window Diameter	6.1 MM
Diode Length (Minus leads)	4.2 MM
Diode Length (Plus leads)	<24.2 MM

The photodiodes produce a current signal which is directly proportional to the amount of incident radiation striking the active area. This current signal is converted to a voltage signal through the use of a current to voltage amplifier. The amplifier design is shown in Figure 7.

Data were recorded by a Campbell Scientific Inc. CR-21 Micrologger. The micrologger was programmed to record once each minute the millivolt signals of the pyranometer and pyrhelimeter and the voltage signals of the photodiodes. The data were then transferred to cassette tape for storage and later processing.

## 2.2 Calibration

The pyrhelimeter was calibrated by Eppley Laboratories and was found to have a sensitivity of .00739 MV/W-M<sup>-2</sup>. The pyranometer was calibrated at the NOAA/Environmental Research Laboratories in Boulder, Colorado, prior to the summer MONEX of 1979. It was found to have a sensitivity of .00857 MV/W-M<sup>-2</sup> and consistent with the pyrhelimeter calibration. A clear dry day was chosen to perform a system calibration for the photodiodes. The 2° field of view instrument was chosen as a "standard" and the other four diodes were compared with

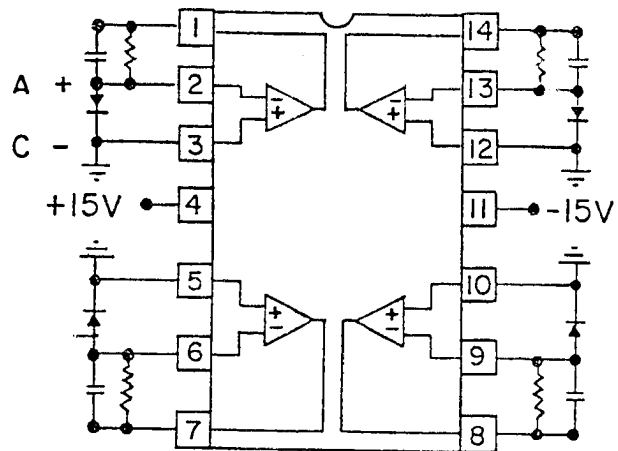


Figure 7. Current to voltage amplifier design including the pin configuration for an MC 47416 chip.

it. Each diode was aimed at the sun without its collimator tube. The outputs of the diodes were recorded by the micrologger for a clear case and for a case where a diffusing plate was present. In this way, diode sensitivities could be determined when both large and small amounts of signal were present. The diode sensitivities were determined by dividing the 2° diode voltage by the voltages from the other four diodes for the diffuse and clear sky cases. The final sensitivity of the diodes was taken to be the average of the diffuse case sensitivity and the clear case sensitivity. The sensitivities determined are given in Table 3.

Table 3. Sensitivities of the photodiodes for the clear case, the diffuse case, and the average sensitivity.

<u>Field of View</u>	<u>Clear</u>	<u>Diffuse</u>	<u>Average</u>
2°	1.000	1.000	1.000
5°	.998	.921	.960
10°	.967	.831	.899
20°	.985	.836	.911
28°	1.0099	1.0061	1.008

### 3.0 RADIATIVE TRANSFER MODEL

#### 3.1 Description

In this application, actual measurements of the angular dispersion of energy from the direct beam in the presence of clouds are compared with results from theoretical computations made with a three dimensional Monte Carlo model. The Monte Carlo model is a multiple scattering model described by McKee and Cox (1974) and Davis, McKee, and Cox (1979). The model was used to determine the amount of energy transmitted through infinite clouds. This model follows the trajectory of photons through a three layer cloud medium and determines the angle of scatter from incidence. To permit the model to simulate a horizontally infinite cloud, any photon exiting the side of a finite volume is reintroduced at a point symmetric with respect to the plane which is parallel to the cloud exit face and which passes through the center of the cloud.

The Monte Carlo model was run for spectral bandpasses of 0.3 to 0.8 and 0.8 to 2.8 microns. The 0.3 to 2.8  $\mu\text{m}$  spectral interval was chosen because it corresponds to the spectral response of the pyrliometer and pyranometer. The U.S. Standard Mid-Latitude Winter Atmosphere of 1962 as presented in McClatchey et al., (1971) is used for the determination of atmospheric effects. Several important parameters must be specified for each spectral region when using the Monte Carlo model. Each spectral region is divided into four wavelength bands. For each wavelength band, a single particle

scattering albedo (SPSA) must be specified. The SPSA is determined from the relationship

$$\text{SPSA} = (\beta_e - \beta_a) / \beta_e \quad (10)$$

where  $\beta_e$  is the volume extinction coefficient and  $\beta_a$  is the volume absorption coefficient. The SPSA is very near unity throughout the entire spectral bandpass. The volume extinction coefficients used in the model are spectrally weighted values determined for each spectral bandpass. The values of  $\beta_a$  and  $\beta_e$  were obtained from Welch, Davis, and Cox (1980). Also entered in the model are the cloud dimensions. The vertical dimension was varied to obtain different cloud geometric and optical depths. Water vapor absorption was determined from the relationship

$$\bar{A} = \frac{1}{\Delta V} [C + D \log_{10} (x + x_o)] \quad (11a)$$

where

$$x = \mu P_{\text{eff}}^{K/D} \quad (11b)$$

and

$$x_o = 10^{-C/D} \quad (11c)$$

The coefficients in the equation were obtained from Liou and Sasamori (1975). Droplet absorption was calculated from the relationship

$$E = E_o W_o \quad (12)$$

where  $E_o$  is the photon's energy before a scatter,  $E$  is the photon's energy after a scatter, and  $W_o$  is the SPSA. The scattering phase function is also specified. Table 4 summarizes other input parameters used in the model.

Table 4. Input parameters used in the Monte Carlo model.

Parameter	Value
Zenith Angle	0°
Azimuth Angle	0°
# of Photons	20000
Max. # of encounters	300

The Legendre expansion coefficients used to specify the single scattering phase function in the model are those given by Zdunkowski (1967) for a Best droplet distribution. The Best droplet distribution has a mean droplet radius of  $10\ \mu\text{m}$ , a liquid water content of  $0.10\ \text{g/m}^3$  and a droplet number concentration of  $100/\text{cm}^{-3}$ . A different set of spectrally weighted Legendre expansion coefficients was used for each spectral bandpass over which the model was run. The Legendre coefficients are used to calculate the scattering phase function which has the form:

$$P(\theta) = 1 + \sum_{n=1}^N \omega_N P_N \cos\theta \quad (13)$$

with  $P_0 = 1$ . The phase function is calculated from  $0^\circ$  to  $1^\circ$  at  $1/100$  degree intervals and from  $1^\circ$  to  $180^\circ$  at  $1/10$  degree intervals. The small interval is used between  $0^\circ$  and  $1^\circ$  because forward scattering dominates and is more important in this region. Figure 8 shows the shape of the scattering functions for the 0.3 to 0.8 and the 0.8 to  $2.8\ \mu\text{m}$  regions. The major difference in the two curves is the stronger forward scattering at shorter wavelengths. For both sets of coefficients, the cumulative probability distribution indicates that at least fifty percent of the scatters which occur will take place at

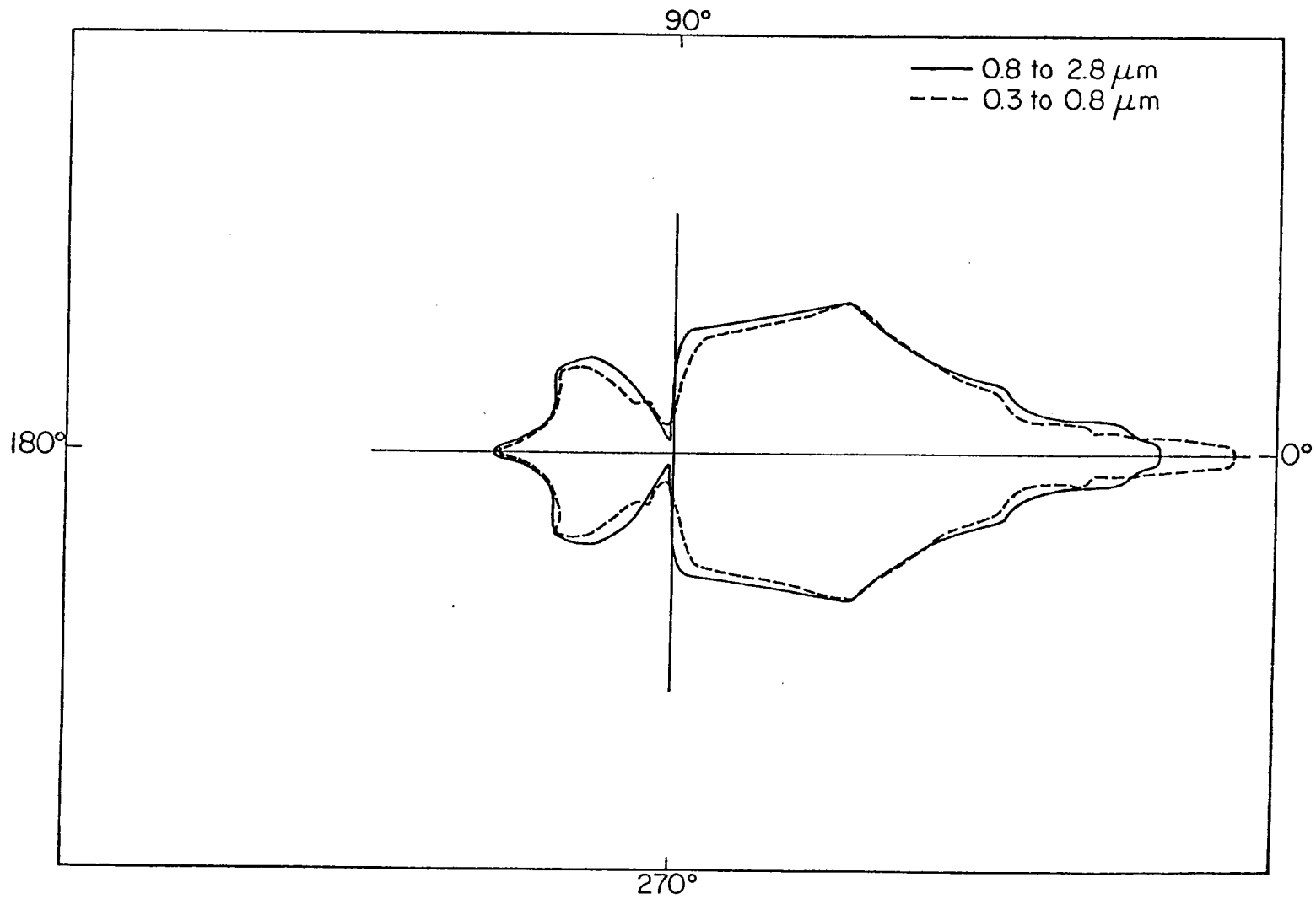


Figure 8. Single scattering phase functions for the two spectral bandpasses used in the MC model.

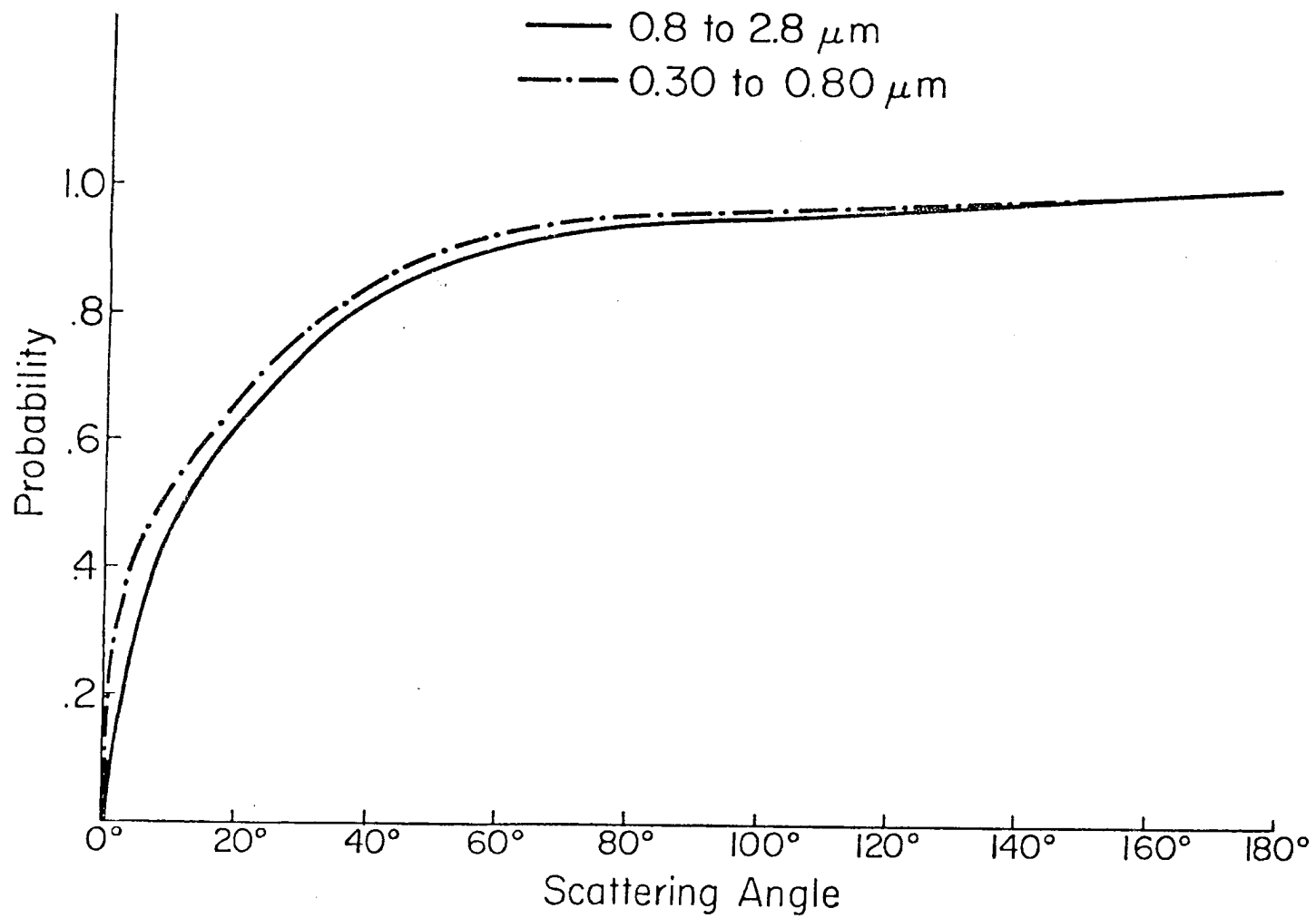


Figure 9. Cumulative probability distribution for both spectral bandpasses used in the MC model.

an angle of  $11.5^\circ$  or less. Figure 9 shows the cumulative probability distribution for both spectral bandpasses.

The Monte Carlo model was run for a variety of cloud optical depths. The cloud optical depth,  $\tau$ , was defined as the cloud thickness multiplied by the volume extinction coefficient. The values of  $\tau$  chosen ranged from 1 to 6. From the relationship

$$I = I_0 e^{-\tau} \quad (14)$$

a  $\tau$  of 6 means that only 50 of the 20000 photons incident at the top of the cloud pass through the cloud without being scattered. From an energy standpoint, the direct solar beam would be reduced from  $1365 \text{ W/M}^2$  at the top of the atmosphere to only  $3.3 \text{ W/M}^2$  at the surface for an atmospheric optical depth of 6. The reasons for choosing a maximum tau of 6 were discussed earlier.

Rayleigh scattering was also neglected when considering model results. Coulson (1975) lists the Rayleigh optical depths for the wavelengths of 0.25 to 1.00 micron at every 0.05 microns. Weighting these values according to the amount of energy incident at each wavelength, the Rayleigh optical depth from 0.25 to 1.00 micron was found to be approximately 0.17. This value is small compared to the values which were used in the model. Above 1.00 micron Rayleigh scattering is negligible.

### 3.2 Model Results

The model output consists of counting the number of photons which exit the base of the cloud at various scattering angles from the incident beam. The scattering angle is determined using the relationship of Kasten and Raschke (1974) which defines the scattering

angle as  $\Psi$  such that

$$\cos \Psi = \cos \theta_i \cos \theta_s + \sin \theta_i \sin \theta_s \cos(\phi_i - \phi_s) \quad (15)$$

where  $\theta_i$  is the angle of incidence,  $\theta_s$  is the angle of scatter from the vertical, and  $\phi_i$  and  $\phi_s$  are the initial and final azimuthal angles.

For a zenith angle of zero, this relationship reduces to

$$\cos \Psi = \cos \theta_s \quad (16)$$

Photons are counted for annular rings with annular widths of  $0-2^\circ$ ,  $2-5^\circ$ ,  $5-10^\circ$ ,  $10-20^\circ$ ,  $20-28^\circ$ , and  $28-180^\circ$ .

The model also determines the amount of energy incident at the top of the atmosphere, the energy which reaches the ground in each annular ring, the energy absorbed by both the atmosphere and the cloud, and the energy leaving the top of the atmosphere. The total amount of transmitted, reflected, and absorbed energy in the  $0.3$  to  $2.8 \mu\text{m}$  spectral bandpass is determined by adding the values obtained in the  $0.3$  to  $0.8$  and  $0.8$  to  $2.8$  micron regions. The energy values obtained for each cloud optical depth are shown in Table 5. A radiance value for each angular band is calculated by dividing the energy in each annular ring by the amount of solid angle in that band. The radiance values are then normalized to the radiance in the  $0-2^\circ$  annulus. The normalized radiances determined at each cloud optical depth are shown in Table 6. Transmittance values are calculated for each full angle field of view, i.e.  $0-2^\circ$ ,  $0-5^\circ$ ,  $0-10^\circ$ , etc., by dividing the energy incident at the surface in a particular field of view by the energy incident at the top of the atmosphere. Table 7 lists the transmittances calculated for each cloud optical depth.

Table 5. Energy values of incident, reflected, absorbed, and transmitted radiation for cloud optical depths of 1 to 6 obtained from the MC model. All energy values are in  $W/M^2$ .

	<u><math>\tau</math></u>					
	<u>1</u>	<u>2</u>	<u>3</u>	<u>4</u>	<u>5</u>	<u>6</u>
Incident	1303	1303	1303	1303	1303	1303
Reflected	66	137	209	271	332	391
Absorbed	184	180	175	170	165	160
Transmitted						
0 - 2°	451	184	79	33	14	6
0 - 5°	538	260	133	65	33	18
0 - 10°	608	331	187	105	61	37
0 - 20°	674	421	261	166	108	77
0 - 28°	719	467	316	215	154	113
0 - 180°	1053	986	919	862	806	752

Table 6. Normalized radiance values calculated for cloud optical depths of 1 to 6.

	<u><math>\tau</math></u>					
	<u>1</u>	<u>2</u>	<u>3</u>	<u>4</u>	<u>5</u>	<u>6</u>
0-2°	1.000	1.000	1.000	1.000	1.000	1.000
2-5°	.037	.078	.130	.187	.267	.356
5-10°	.0082	.021	.037	.064	.111	.152
10-20°	.0020	.0058	.013	.025	.047	.084
20-28°	.0010	.0031	.0073	.016	.035	.059
28-180°	.00025	.00044	.0012	.0031	.0075	.016

Table 7. Transmittance values calculated for cloud optical depths of 1 to 6.

	<u>τ</u>					
	<u>1</u>	<u>2</u>	<u>3</u>	<u>4</u>	<u>5</u>	<u>6</u>
0-2°	.3461	.1414	.0604	.0253	.0104	.0049
0-5°	.4131	.1997	.1017	.0501	.0251	.0141
0-10°	.4667	.2543	.1437	.0804	.0467	.0282
0-20°	.5176	.3162	.2003	.1275	.0832	.0592
0-28°	.5521	.3584	.2423	.1652	.1181	.0870
0-180°	.8080	.7568	.7056	.6616	.6188	.5770

#### 4.0 DATA REDUCTION PROCEDURES

Data from the pyranometer, pyrhelimeter, and photodiode array were collected on several days during the period from October 1981 through April 1982. During the data collection periods, data were collected once a minute and recorded on cassette tape. All-sky photographs were taken on some of the data collection days. Table 8 is a summary of the sky conditions on data collection days.

#### DATA COLLECTION LOG

Table 8. Summary of the sky conditions on data collection days. The precipitable water values are those given for Denver, Colorado, and were taken from NMC facsimile charts. NA indicates not available.

<u>Day</u>	<u>Time (MST)</u>	<u>Cloud Cover</u>	<u>Precip. Water (cm)</u>	
10/19/81	810-1554	Clear all day	1200Z	.20
10/20/81	842-1545	Very thin cirrus during the morning. More dense during one period after noon.	1200Z	.23
10/26/81	1041-1632	Extensive cirrus along with some mountain wave clouds	1200Z 0000Z	.36 .64
10/27/81	1401-1630	Sky mostly clear except for small lenticulars. Cirrus on western horizon.	1200Z	.46

10/28/81	943-1615	Mostly clear early morning. Extensive cirrus mid-day. Altcumulus during afternoon.	1200Z 0000Z	.46 1.09
11/9/81	1043-1609	Sky clear, some haze	1200Z 0000Z	.66 .36
11/10/81	1001-1609	Sky clear	NA	
11/13/81	800-1554	Altcumulus in the morning. Cirrus, cirrostratus, and cirrocumulus during the afternoon.	1200Z	.43
11/23/81	1001-1400	Mostly altcumulus through entire period	NA	
1/12/82	822-1615	Dense stratus in the morning with some snow falling. Stratus thins as day progresses. Scattered stratus and some cirrus during afternoon.	1200Z	1.14
1/15/82	934-1620	Mostly thin cirrus during the day.	NA	
1/18/82	949-1600	Extensive cirrus in the morning. Less dense in the afternoon.	NA	
2/18/82	1115-1645	Mostly clear until late afternoon when extensive altcumulus are present.	NA	
2/22/82	1037-1645	Cirrus and altostratus present through most of the period. Some lenticulars are also present.	NA	
4/15/82	1400-1545	Cumulus and glaciated cumulus during entire period.	NA	

The millivolt signals from the pyrliometer and pyranometer were divided by the instrument sensitivity to obtain an irradiance value in

$W/M^2$ . The voltages from the photodiodes were initially multiplied by the sensitivities listed in Table 3 to obtain corrected voltages. Irradiance values for the photodiodes were then calculated. The voltage of the  $5^\circ$  field of view diode was allowed to correspond to the irradiance value of the pyrhelimeter. This was done because the pyrhelimeter has a field of view which is very near five degrees. The irradiance values for the  $2^\circ$ ,  $10^\circ$ ,  $20^\circ$ , and  $28^\circ$  field of view diodes were then calculated by using the method shown in Equations 17 and 18.

$$\frac{5^\circ \text{ Voltage}}{\text{FOV Voltage}} = \frac{5^\circ \text{ Irradiance}}{\text{FOV Irradiance}} \quad (17)$$

$$\text{FOV Irradiance} = \frac{\text{FOV Voltage}}{5^\circ \text{ Voltage}} \times 5^\circ \text{ Irradiance} \quad (18)$$

Transmittance values for each field of view could then be determined by dividing the irradiances by the solar constant which is defined to be  $1303 W/M^2$  for the 0.3 to 2.8 micron region. These transmittances could then be compared to those found from the Monte Carlo model. Radiance values for the annular rings of  $0-2^\circ$ ,  $2-5^\circ$ ,  $5-10^\circ$ ,  $10-20^\circ$ , and  $20-28^\circ$  were calculated by first finding the irradiance in each band and then dividing by the appropriate solid angle. The radiance values were then normalized to the  $2^\circ$  field of view value. These normalized radiances could also be compared to results obtained from the Monte Carlo model.

## 5.0 COMPARISON OF MODEL AND EXPERIMENTAL RESULTS

### 5.1 Procedures

Two methods are used to compare actual measurements made with the photodiodes to the results obtained from the Monte Carlo radiative transfer model. First, model values of transmittance are compared graphically with experimental values. Values of transmittance versus field of view are plotted for cloud optical depths of 1 through 6. One minute instantaneous and ten minute average values of transmittance obtained from the photodiodes are then plotted and compared to the model values.

The second method of comparison involves an attempt to relate transmittance mathematically to optical depth. Two types of mathematical comparisons are made. First, the values of transmittance obtained from the Monte Carlo model were inserted into a Givens matrix rotation routine similar to the one described by Noble (1969) in order to obtain a single equation relating optical depth to the transmittances from the five fields of view. The resulting equation has the form:

$$\tau = A_0 + A_1 \ln T_2 + A_2 \ln T_5 + A_3 \ln T_{10} + A_4 \ln T_{20} + A_5 \ln T_{28} \quad (19)$$

where the T's are the transmittance values for the given fields of view. The values of the coefficients in Equation (19) are given in Table 9. Using the model transmittances, the equation

predicts optical depths which agree very well with the expected values as shown in Table 10.

Table 9. Values of the Coefficients in Equation 19.

<u>Coefficient</u>	<u>Value</u>
$A_0$	- .15402
$A_1$	1.13013
$A_2$	2.39880
$A_3$	- 4.13540
$A_4$	- .26406
$A_5$	2.10386

Table 10. Calculated versus expected values of  $\tau$  using model transmittances and Equation 19.

<u>Expected</u>	<u>Calculated</u>
1	.999994
2	1.999969
3	2.999989
4	3.999978
5	4.999969
6	5.999948

If the transmittance is related to optical depth by an exponential function,

$$T = e^{-\tau} \quad (20)$$

the transmittance for a particular field of view, J, can be written as

$$T_J = e^{-\tau_J} \quad (21)$$

Using this relation, Equation 19 can be written in the form:

$$\tau = A_0 + A_1 \ln e^{-\tau_2} + A_2 \ln e^{-\tau_5} + A_3 \ln e^{-\tau_{10}} + A_4 \ln e^{-\tau_{20}} + A_5 \ln e^{-\tau_{28}} \quad (22)$$

or

$$\tau = A_0 + A_1(-\tau_2) + A_2(-\tau_5) + A_3(-\tau_{10}) + A_4(-\tau_{20}) + A_5(-\tau_{28}) \quad (23)$$

In essence then, Equation 23 indicates that the optical depth  $\tau$  is just a weighted average of the optical depths calculated at each field of view.

A second method of calculated optical depth was obtained by first plotting optical depth versus transmittance for each field of view. These plots are shown in Figure 10. To relate transmittance to optical depth, an equation was then found for each of the curves in Figure 10. The equations of the curves yield a value of optical depth for each of the five fields of view when the transmittance values for each FOV are inserted. The optical depth of the cloud is then taken to be the average value of the five optical depths predicted by the equations. The equations of the curves of Figure 10 have the form

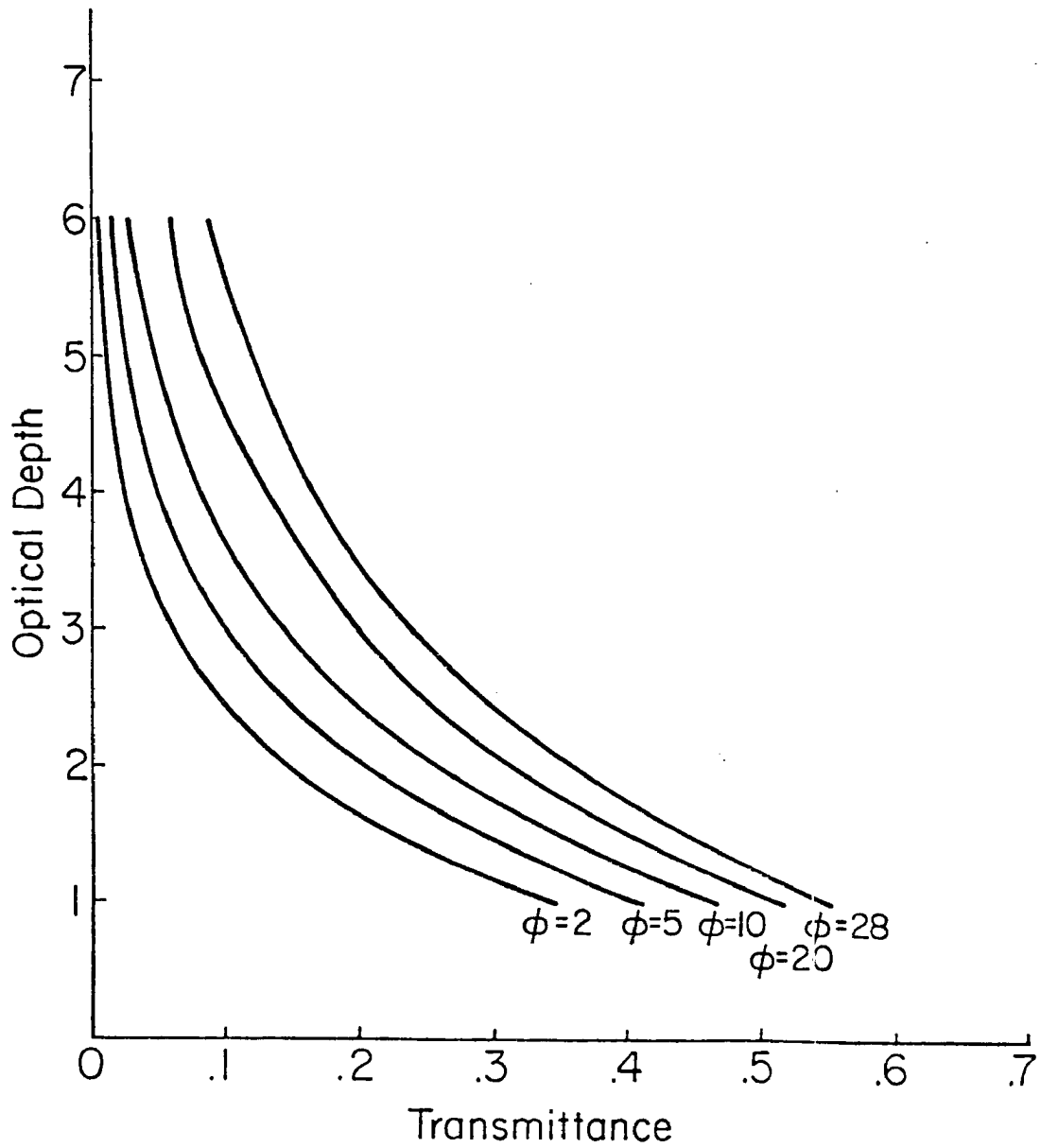


Figure 10. Optical depth versus transmittance for 2°, 5°, 10°, 20°, and 28° fields of view produced from the Monte Carlo model.

$$y = a + b \ln x \quad (24)$$

where  $x$  is the transmittance for a given field of view and  $y$  is the optical depth. The  $a$  and  $b$  coefficients of Equation 24 are listed in Table 11.

Table 11. Coefficients of the curves relating transmittance to optical depth for the five fields of view. The equations have the form  $y = a + b \ln x$ .

<u>FOV</u>	<u>a</u>	<u>b</u>	<u>Corr. Coeff.</u>
2°	-.26906	-1.1666	.99948
5°	-.34655	-1.4681	.99901
10°	-.41304	-1.7754	.99911
20°	-.58852	-2.2697	.99763
28°	-.72527	-2.6923	.99634

Again, both instantaneous and ten minute average values of transmittance are used to calculate the cloud optical depths.

Next we need an evaluation procedure to determine how well the calculated optical depths agree with the graphical predictions. Using the equations of the curves in Figure 10, values of transmittance which would be produced by the Monte Carlo model can be calculated for optical depths close to the experimental value. To determine if the calculated  $\tau$  values are really representative of the data points, the optical depth producing the smallest root mean square error between the calculated and experimental transmittances is found. The smallest RMS error indicates the model curve which best fits the experimental values.

Similar calculations were made using the normalized radiance values. The equations of the curves of normalized radiance versus optical depth frequently produced a much wider range in the calculated optical depths than was produced by the equations using transmittance. For this reason, only the results obtained using the transmittance values will be discussed in the case studies which follow.

## 5.2 Case Studies

The following sections examine representative data collected during periods when high, middle, or low clouds were present.

### 5.21 High Clouds

The following four cases compare the experimental results obtained with varying optical thicknesses of mainly cirrus, cirrostratus, or cirrocumulus to the Monte Carlo model results. In making this comparison, one should keep in mind that while high clouds consist mainly of ice, the model was run using water clouds.

October 28, 1981            1055 - 1104 MST

Figure 11a shows the cloud cover present at this time. A relatively uniform cirrus or cirrostratus layer is located to the south with the sun behind its northern fringes. Much thinner cirrus is located to the north.

The transmittance values for 1100 MST are shown by the X's in Figure 12a. These points indicate an optical depth which is close to, but slightly less than one. The 10 minute average values of transmittance for the period 1055-1104 MST are plotted in Figure 12b. These points show an optical depth which is both less than one and less than the instantaneous case. In both the instantaneous and



Figure 11a. Photograph of cloud cover at 1100 MST October 28, 1981.



Figure 11b. Photograph of cloud cover at 1220 MST October 26, 1981.



Figure 11c. Photograph of cloud cover at 1040 MST November 13, 1981.

1100MST October 28, 1981

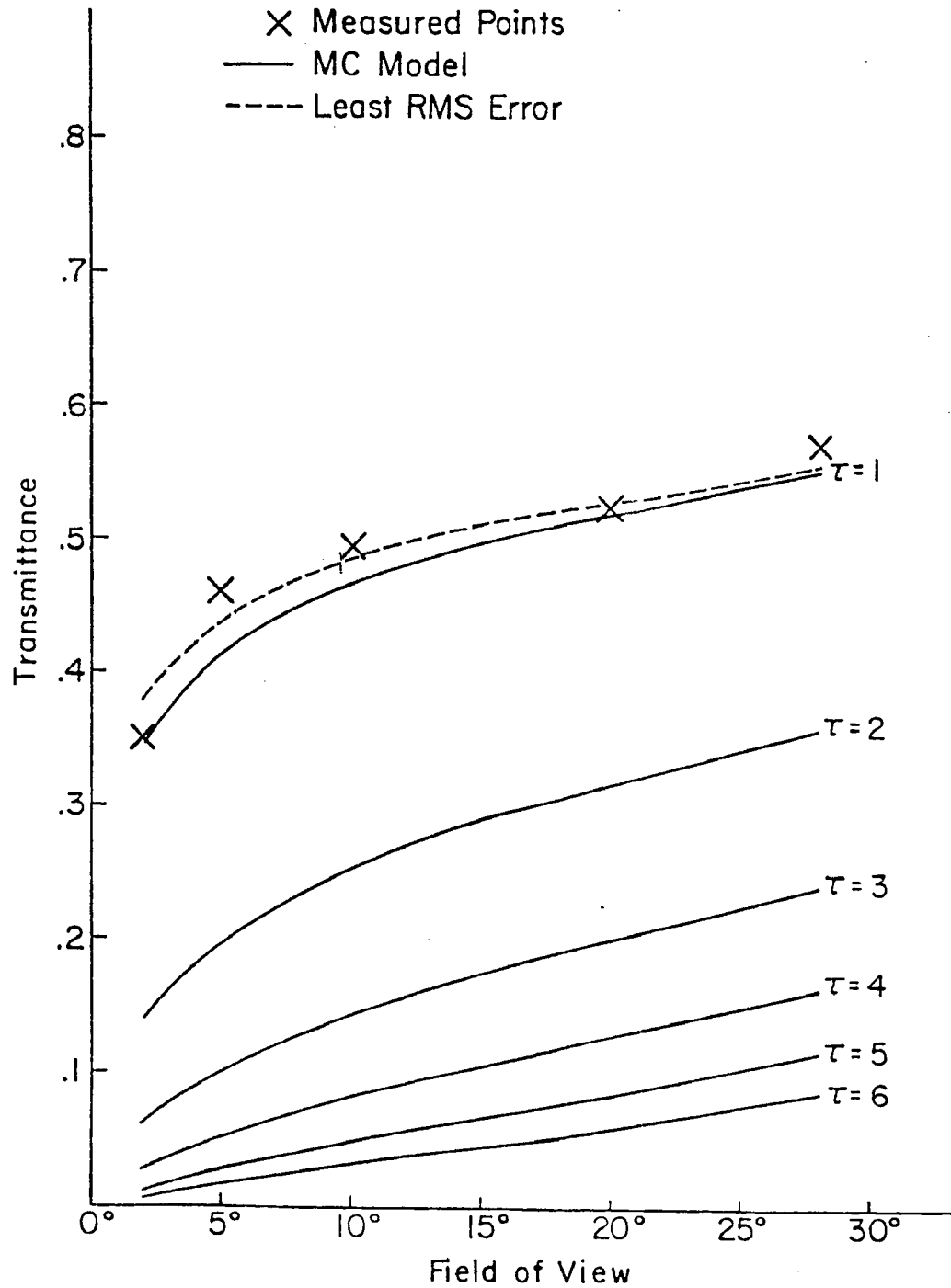


Figure 12a. Transmittance versus field of view for 1100 MST October 28, 1981.

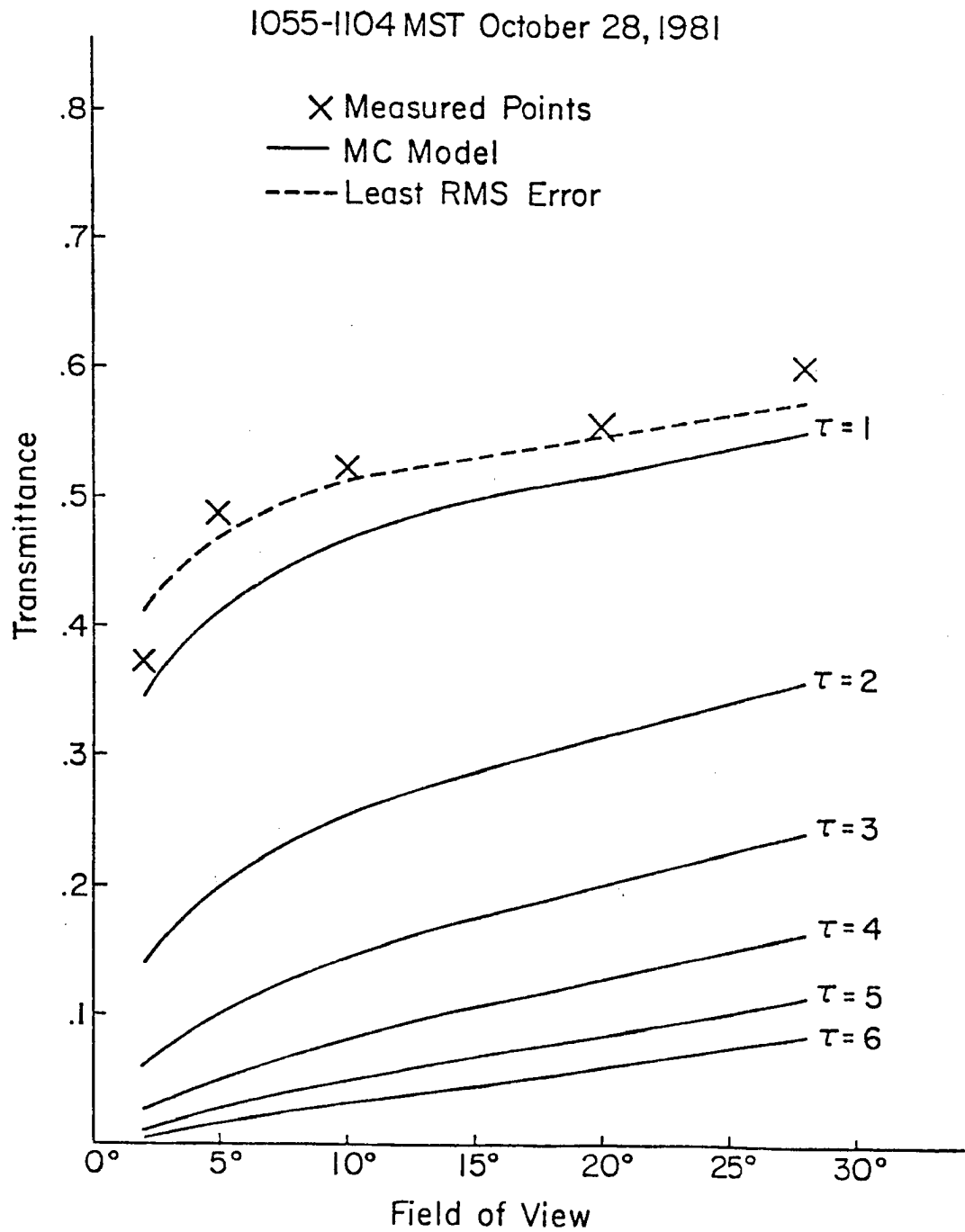


Figure 12b. Ten minute average values of transmittance versus field of view for the period 1055-1104 MST October 28, 1981.

average cases, the profile shapes suggested by the data points show good agreement with the model curves.

Table 12 shows the calculated optical depths for the October 28th case. The second column of Table 12 (labeled  $\tau_{EQ}$ ) shows the optical depths determined for both the one minute and ten minute periods using Equation 19. The next six columns show the optical depths calculated at each field of view and the average FOV optical depth for the one minute and ten minute periods.

Table 12. Calculated optical depths for the period 1055-1104 MST October 28, 1981.

TIME	$\tau_{EQ}$	$\tau_2$	$\tau_5$	$\tau_{10}$	$\tau_{20}$	$\tau_{28}$	$\tau_{AVE}$	$\sigma$
1055	1.02	.88	.69	.73	.74	.62	.73	.095
1056	.93	.76	.55	.58	.58	.43	.58	.118
1057	.97	.80	.59	.62	.62	.48	.62	.115
1058	.87	.74	.57	.58	.58	.42	.58	.113
1059	1.01	.88	.72	.75	.78	.66	.76	.081
1100	1.07	.95	.80	.84	.89	.78	.85	.069
1101	1.08	.96	.80	.84	.88	.78	.85	.072
1102	1.02	.89	.72	.75	.73	.65	.76	.088
1103	1.06	.93	.76	.80	.83	.71	.81	.083
1104	1.17	1.07	.91	.96	1.02	.94	.98	.064
1055- 1104	1.02	.89	.71	.75	.77	.65	.75	.089
1055- 1104	1.02	.89	.71	.74	.77	.64	.75	.092

The last column shows the standard deviation ( $\sigma$ ) about the average. The difference between the two rows of ten minute average values will be discussed later. At 1100 MST, Equation 19 predicts an optical depth of 1.07. This value is somewhat higher than predicted by the points in Figure 12a. Using the average value of the optical depth calculated at each field of view, a  $\tau$  of 0.85 is obtained. This is more in line with what is shown in Figure 12a. The ten minute average values of transmittance also predict a larger value of  $\tau$  using Equation 19 than when using the average FOV optical depth. Again, the average FOV optical depth shows much better agreement with the points in Figure 12b. The model optical depths which produce the smallest RMS errors for the instantaneous and average cases are 0.86 and 0.77 respectively. The model curves corresponding to these two  $\tau$  values are shown by the dashed lines in Figures 12a and 12b. This indicates that the average FOV optical depth more accurately represents the cloud optical depth in this case.

Also of note for this case is the fact that  $\tau$  values are very similar throughout the ten minute period indicating that the thickness of the cloud field changed only slightly. That some inhomogeneities exist in the cloud field is shown by the variability of the standard deviations. The largest  $\sigma$  occurs at 1056 MST and has a value of .118. The FOV optical depths range from .43 to .76 with a difference of .33. The smallest standard deviation is .064 and corresponds to a maximum spread of  $\tau$  values which is only 0.16. The largest  $\sigma$ 's occur in the first five minutes of the case study period and are probably a result of the sun being located in the thinner, more broken cirrus field at this time. The smaller optical depths support this contention. The

$\sigma$ 's are generally lower in the last five minutes of the period due to the effect of the more uniform cirrostratus field on the scattering taking place.

October 26, 1981            1216-1225 MST

The cloud cover for this period is shown in Figure 11b. The sun is located in a moderately thick cirrocumulus layer with dense altocumulus to the southwest. This cloud cover appeared visually more dense than the October 28th case.

Figure 12c shows the plot of transmittance versus field of view for 1220 MST. The plotted points indicate an optical depth between 2.5 and 3. The average transmittance values for 1216-1225 MST are shown in Figure 12d. These points indicate a smaller optical depth probably around 2.5. These points seem to show less agreement with the model curves than the previous case.

The calculated optical depths for this case are shown in Table 13. For 1220 MST, Equation 19 predicts a  $\tau$  of 2.81 while the average FOV  $\tau$  was found to be 2.71. Again, Equation 19 predicts the higher optical depth of the two methods of calculation but the difference is less than the October 28th case. For the period 1216-1225 MST, Equation 19 produces an optical depth of 2.49 which compares favorably with a value of 2.44 from the FOV transmittances. These calculated values also agree with the plotted points in Figures 12c and 12d. The model optical depths which produce the smallest RMS errors for these two periods and which agree very well with the calculated values are 2.77 and 2.44 respectively. The field of view versus transmittance curves producing the smallest RMS errors with experimental data are shown by the dashed lines in Figures 12c and 12d.

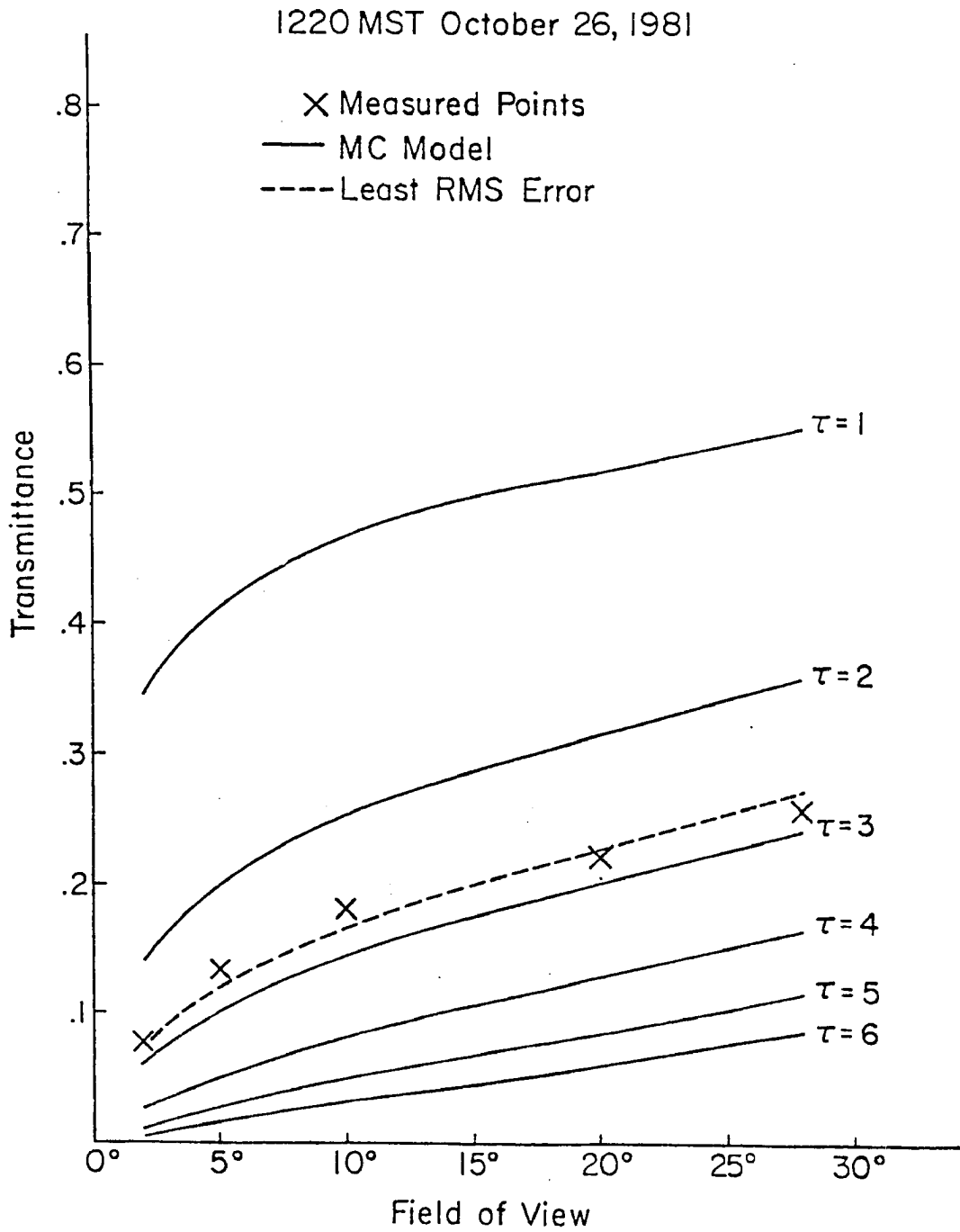


Figure 12c. Transmittance versus field of view for 1220 MST October 26, 1981.

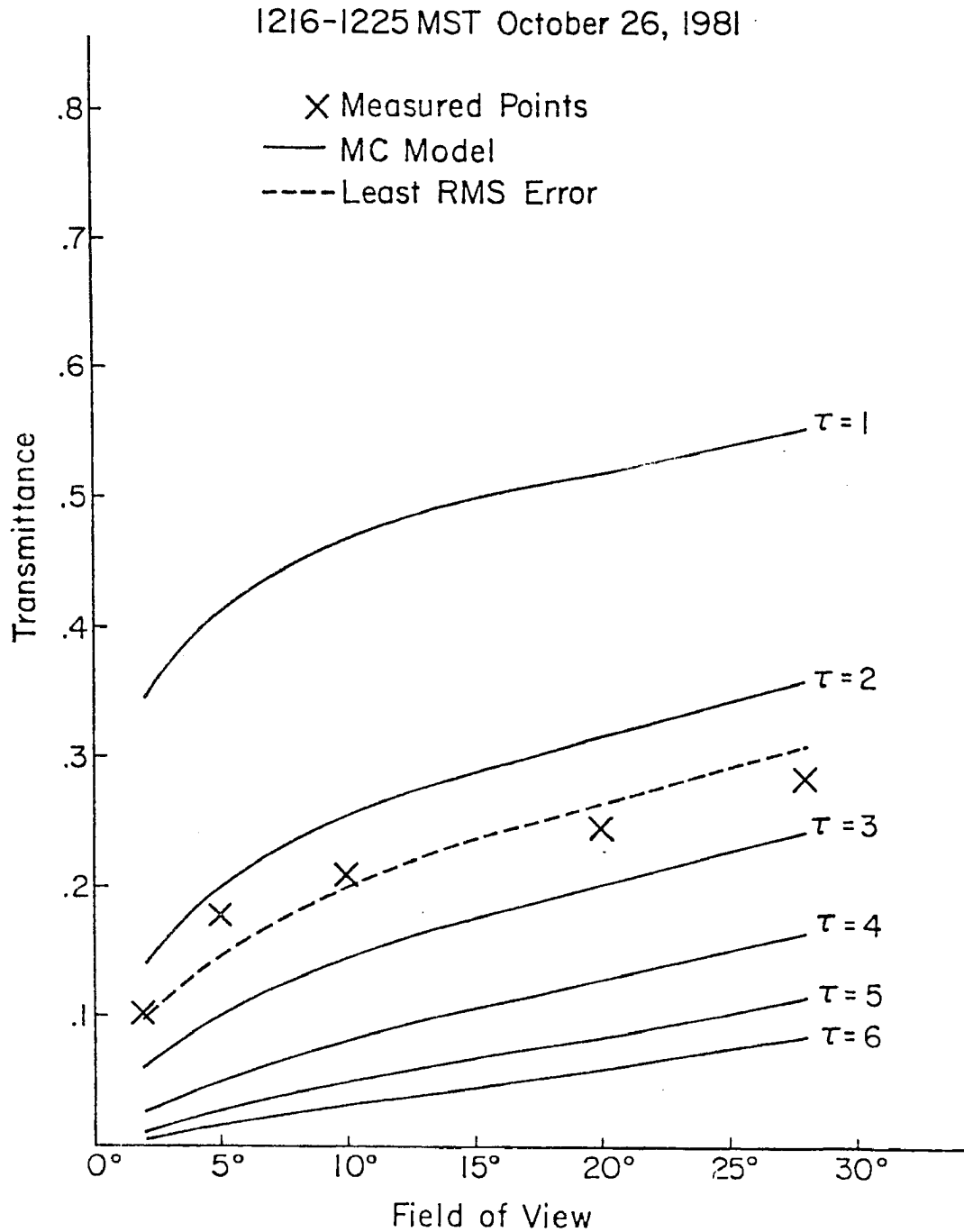


Figure 12d. Ten minute average values of transmittance versus field of view for the period 1216-1225 MST October 26, 1981.

For this ten minute period, cloud optical depth changes much more from minute to minute than the previous case. Optical depth values range from 1.58 to 3.45 indicating significant variations in cloud thickness exist for this cloud field.

Table 13. Calculated optical depths for the period 1216-1225 MST October 26, 1981.

TIME	$\tau_{EQ}$	$\tau_2$	$\tau_5$	$\tau_{10}$	$\tau_{20}$	$\tau_{28}$	$\tau_{AVE}$	$\sigma$
1216	3.47	3.40	3.10	3.34	3.62	3.78	3.45	.262
1217	2.64	2.54	2.29	2.50	2.74	2.85	2.58	.218
1218	2.57	2.45	2.20	2.43	2.69	2.79	2.51	.215
1219	2.82	2.73	2.42	2.63	2.88	2.99	2.73	.221
1220	2.81	2.72	2.42	2.62	2.84	2.94	2.71	.201
1221	2.68	2.57	2.30	2.51	2.73	2.83	2.59	.205
1222	1.95	1.76	1.41	1.54	1.61	1.57	1.58	.126
1223	1.97	1.84	1.70	1.83	1.98	1.97	1.86	.116
1224	2.30	2.19	2.10	2.28	2.50	2.56	2.33	.198
1225	2.50	2.37	2.41	2.63	2.89	2.98	2.66	.248
1216-								
1225	2.57	2.46	2.24	2.43	2.65	2.73	2.50	.193
1216-								
1225	2.49	2.37	2.17	2.37	2.59	2.66	2.43	.195

The standard deviations are also much larger for this time period with the exception being 1223 MST. The largest  $\sigma$  value was .262 at 1216 MST with a  $\tau_{\text{MAX}} - \tau_{\text{MIN}}$  value of .68. The smallest optical depth was .116 at 1223 MST and corresponded to a maximum difference in FOV optical depths of .28. The larger  $\sigma$ 's indicate that the cloud field for this case is less uniform than the previous case. As the points in both Figures 12c and 12d show, the small fields of view show a smaller optical depth and the large fields of view indicate a greater optical depth than expected by the RMS best fit curves. This too is probably due to the nonuniformity of cloud the field. The larger optical depths predicted by the wide fields of view may be due to some effect of the dense altocumulus layer which was present in the surrounding area.

November 13, 1981            1036-1045 MST

The cloud field present at this time is shown in Figure 11c. A moderately thick cirrostratus layer is covering the sun. This cloud appears to be fairly uniform near the sun and clear areas exist to the west. The thickness of the cloud appears to be slightly greater than the October 26th case.

Figure 12e shows the plot of transmittance versus field view for 1040 MST. The data points in this figure predict an optical depth between 3.25 and 3.5. The plot of ten minute average values of transmittance in Figure 12f is very similar to the one minute value curve and also predicts an optical depth between 3.25 and 3.5. The points in these curves show agreement with the model curves which is comparable to the previous case.

Table 14 lists the calculated optical depths for this cloud case. At 1040 MST, Equation 19 predicts a  $\tau$  value of 3.32 while the average FOV  $\tau$  value for this period is calculated to be 3.40. For the ten minute period, the equation suggests a  $\tau$  of 3.29 while the average from the five fields of view is 3.39. For this case, the equation predicts a smaller  $\tau$  value than what is obtained using the average. This is in direct contrast to what occurred for the previous two cases. Again, however, the differences in the two values are relatively minor. As before, the calculated values agree very well with the plotted points.

Table 14. Calculated optical depths for the period 1036-1045 MST  
November 13, 1981.

TIME	$\tau_{EQ}$	$\tau_2$	$\tau_5$	$\tau_{10}$	$\tau_{20}$	$\tau_{28}$	$\tau_{AVE}$	$\sigma$
1036	2.00	2.02	1.86	1.90	2.03	2.01	1.96	.078
1037	2.85	2.95	2.74	2.76	2.91	2.96	2.86	.106
1038	3.26	3.41	3.11	3.07	3.17	3.19	3.19	.132
1039	3.18	3.25	3.06	3.10	3.24	3.27	3.18	.097
1040	3.32	3.38	3.23	3.31	3.50	3.58	3.40	.138
1041	3.52	3.62	3.49	3.54	3.72	3.79	3.63	.124
1042	4.25	4.30	4.15	4.18	4.24	4.30	4.23	.069
1043	4.57	4.67	4.54	4.54	4.61	4.67	4.61	.065
1044	4.07	4.09	4.07	4.23	4.50	4.64	4.31	.254
1045	4.34	4.39	4.29	4.39	4.54	4.68	4.46	.154
<hr/>								
1036-								
1045	3.54	3.61	3.45	3.50	3.65	3.71	3.58	.107
<hr/>								
1036-								
1045	3.29	3.34	3.23	3.31	3.50	3.57	3.39	.141

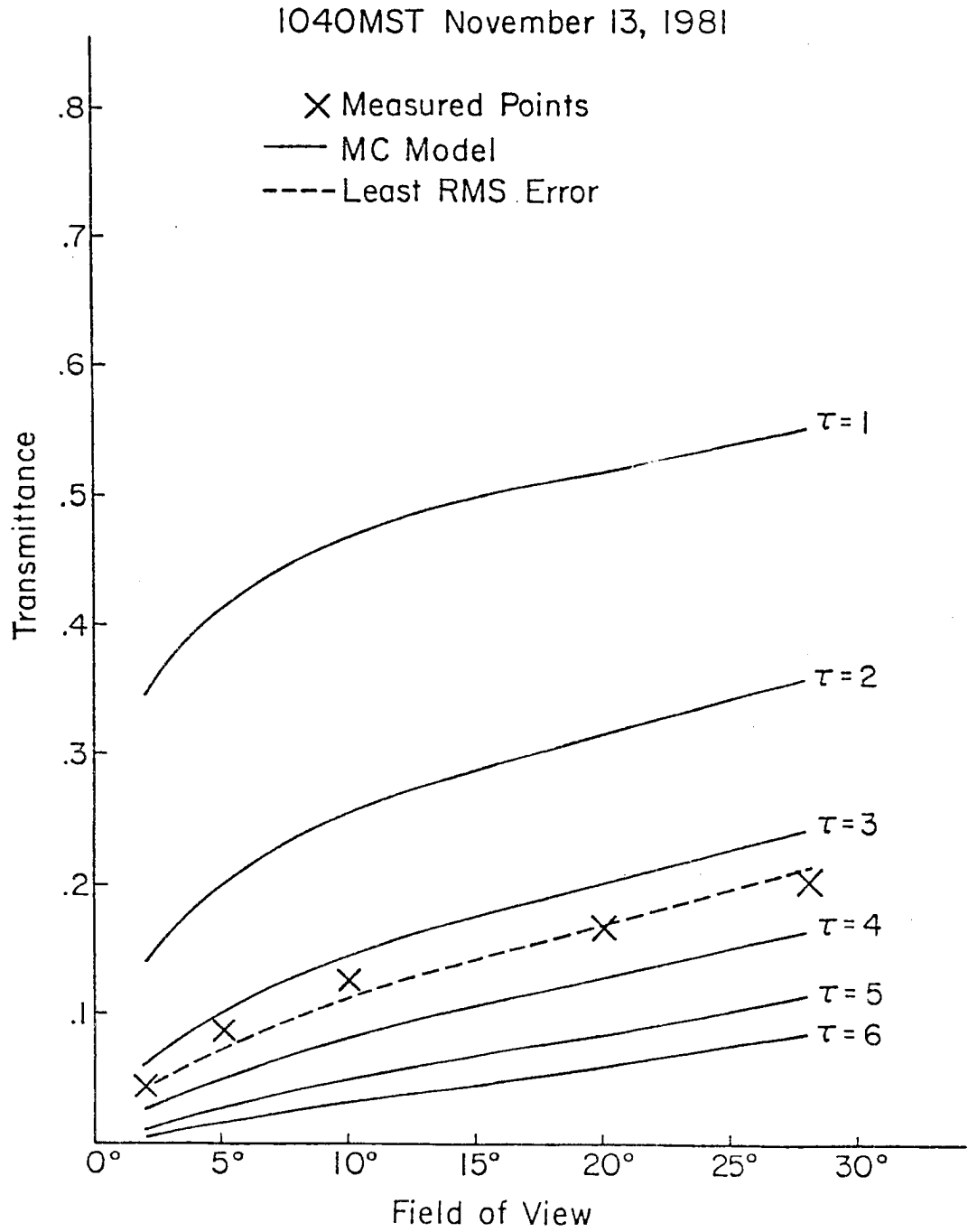


Figure 12e. Transmittance versus field of view for 1040 MST November 13, 1981.

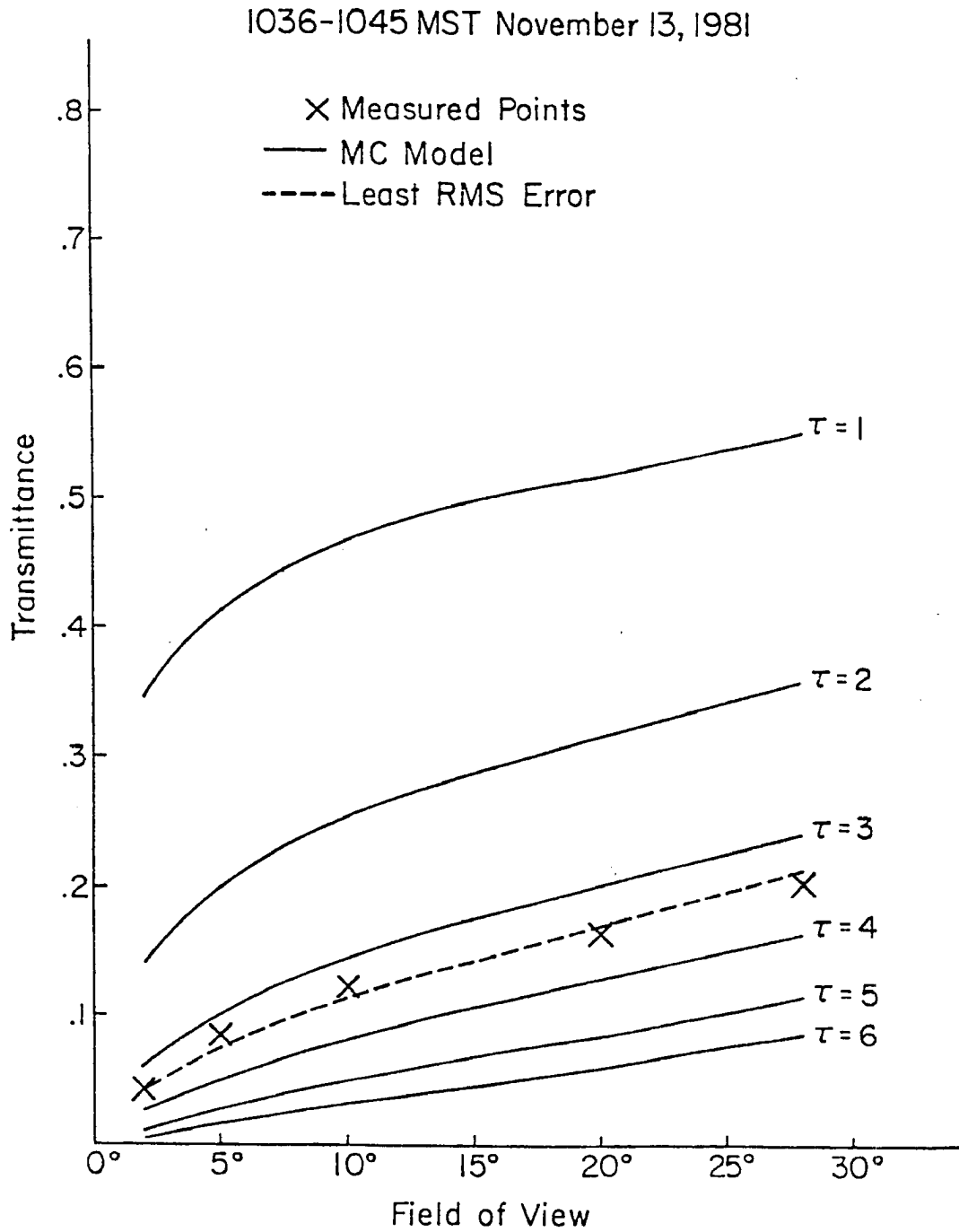


Figure 12f. Ten minute average values of transmittance versus field of view for the period 1036-1045 MST November 13, 1981.

The dashed lines in Figures 12e and 12f correspond to the model optical depths producing the smallest RMS errors with experimental data. These optical depths were 3.44 for 1040 MST and 3.43 for 1036-1045 MST. The  $\tau$  value producing the smallest RMS error again agrees more closely with the average FOV optical depth than with the value from Equation 19.

As with the October 26th case, the optical depth of the cloud field changes significantly during the ten minute period.  $\tau$  increased steadily through the period indicating an increase in cloud thickness. The range of standard deviations for this case is greater than for the previous two cases. Values range from .065 at 1043 MST to .254 at 1044 MST indicating that the cloud field was probably not as uniform in nature as Figure 11c would indicate. This is especially true during the end of the ten minute period when the clear areas may be causing a decrease in the energy reaching the wide fields of view. Like the October 26th case, the plotted points in Figures 12e and 12f show less energy reaching the wide fields of view and more energy reaching the narrow fields of view than predicted by the model curves. The difference between model and experiment is less in this case than the previous case, however.

February 22, 1982      1216-1225 MST

For the final high cloud case, the sun is behind a cirrostratus layer which is optically thicker than the previous three cloud fields. No photographs were taken on this day.

Experimental values of transmittance measured at 1221 MST are shown in Figure 12g. The data points indicate an optical depth which is between 5.5 and 6. The ten minute average values of transmittance

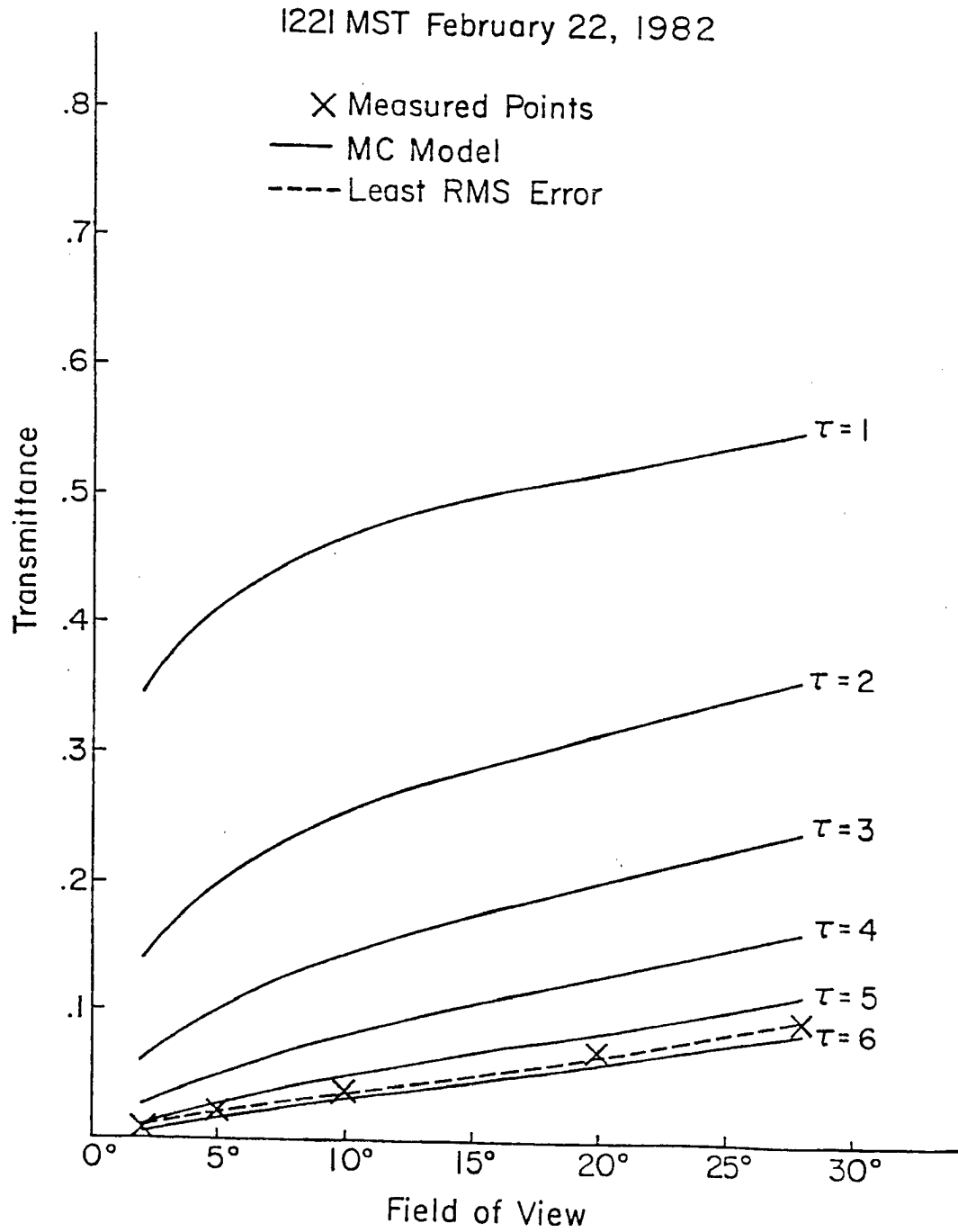


Figure 12g. Transmittance versus field of view for 1221 MST February 22, 1982.

1216-1225 MST February 22, 1982

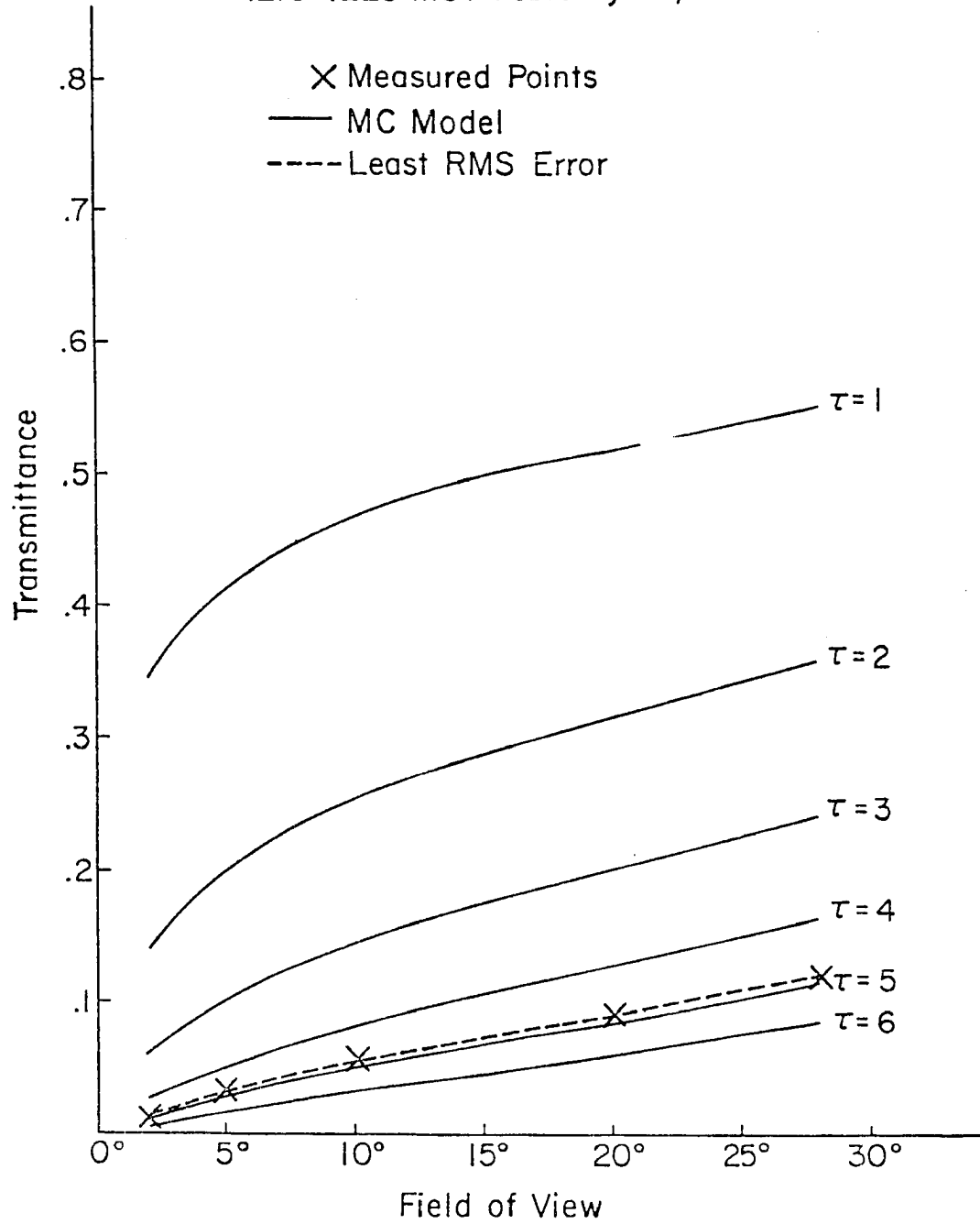


Figure 12h. Ten minute average values of transmittance versus field of view for the period 1216-1225 MST February 22, 1982.

The ten minute average values of  $\tau$  were found to be 4.77 and 4.93 from the two methods. Again, Equation 19 predicts a smaller  $\tau$  value than the averaging method. The model optical depths producing the best RMS fits to the experimental data were 5.57 and 4.96 for the one and ten minute periods. These values agree very well with the calculated values in Table 15 and also with what was predicted in Figures 12g and 12h.

The variability of the cloud optical depth for the February 22nd case was somewhat less than the two previous cases. Values of  $\tau$  ranged from 4.61 to 5.65 with a ten minute average value of 4.93. This indicates that the cloud cover was quite thick through the entire period. The variability in the optical depths calculated at each field of view is about the same as the previous cases. Standard deviations run from .072 at 1221 MST to .184 at 1224 MST again indicating that some nonuniformities do exist in the cloud field. Also indicating the variance of the cloud field is the fact the optical depth varies randomly from minute to minute. Unlike the previous cases, the wide fields of view do not always predict a larger optical depth than expected and the small fields of view do not always predict a smaller optical depth than expected. This trend does show up to some extent in the ten minute average values, however.

#### 5.22 Mid-level Clouds

November 23, 1981            1021-1030 MST

The November 23rd case is the only mid-level cloud situation considered. The photograph of cloud cover at 1030 MST is shown in Figure 13. The sun is in a large area of moderately dense altocumulus which is rather nonuniform and contains quite a few breaks.

are shown in Figure 12h. The average optical depth for 1216-1225 MST appears to be between 4.75 and 5.00. As with previous cases, the data points show good agreement with the model curves.

The mathematically determined optical depths for the February 22nd case are shown in Table 15. At 1221 MST, Equation 19 produces an optical depth of 5.44. This compares with a value of 5.58 from the average of the five field of view optical depths.

Table 15. Calculated optical depths for the period 1216-1225 MST February 22, 1982.

TIME	$\tau_{EQ}$	$\tau_2$	$\tau_5$	$\tau_{10}$	$\tau_{20}$	$\tau_{28}$	$\tau_{AVE}$	$\sigma$
1216	4.60	4.90	4.56	4.50	4.66	4.75	4.67	.158
1217	4.64	4.96	4.77	4.69	4.84	4.94	4.84	.114
1218	4.74	4.99	4.72	4.68	4.81	4.92	4.82	.131
1219	4.45	4.76	4.46	4.43	4.64	4.78	4.61	.164
1220	4.47	4.79	4.50	4.48	4.74	4.87	4.68	.176
1221	5.44	5.67	5.58	5.50	5.51	5.62	5.58	.072
1222	5.57	5.74	5.58	5.55	5.64	5.74	5.65	.088
1223	5.20	5.31	5.07	5.03	5.16	5.28	5.17	.124
1224	4.49	4.80	4.54	4.53	4.81	4.95	4.73	.284
1225	4.71	4.94	4.77	4.76	4.93	5.05	4.89	.123
<hr/>								
1216-								
1225	4.83	5.09	4.86	4.82	4.97	5.09	4.97	.126
<hr/>								
1216-								
1225	4.77	5.04	4.81	4.77	4.95	5.07	4.93	.134

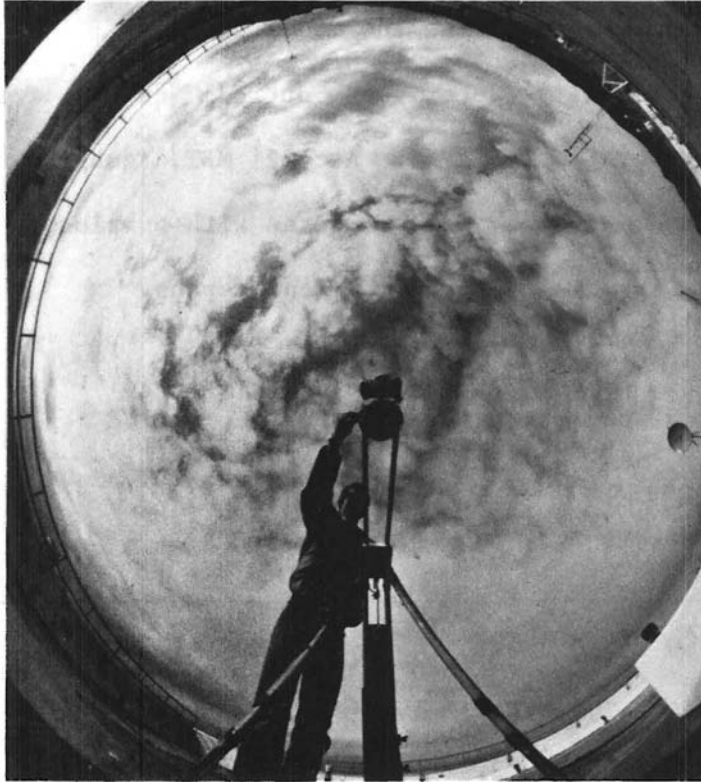


Figure 13. Photograph of cloud cover at 1030 MST November 23, 1981.

Figure 14a shows the plot of the experimental data for 1025 MST. These transmittance values predict an optical depth near 2.5 and show good agreement with the model curves. The ten minute average values of transmittance in Figure 14b predict an optical depth of approximately 1.9. These data points show less agreement with the model curves than the one minute case.

Calculated optical depths for 1021-1030 MST are shown in Table 16.

Table 16. Calculated optical depths for the period  
1021-1030 MST November 23, 1981.

TIME	$\tau_{TQ}$	$\tau_2$	$\tau_5$	$\tau_{10}$	$\tau_{20}$	$\tau_{28}$	$\tau_{AVE}$	$\sigma$
1021	1.72	1.69	1.62	1.66	1.70	1.71	1.68	.037
1022	1.96	1.97	1.92	1.99	2.07	2.17	2.02	.098
1023	1.69	1.66	1.61	1.69	1.72	1.82	1.70	.078
1024	.83	.73	.59	.58	.53	.43	.57	.109
1025	2.45	2.51	2.44	2.48	2.49	2.65	2.51	.080
1026	3.06	3.18	3.05	3.06	3.03	3.24	3.11	.093
1027	3.43	3.68	3.54	3.49	3.43	3.69	3.57	.116
1028	2.49	2.48	2.54	2.73	2.92	3.16	2.77	.280
1029	1.63	1.57	1.54	1.60	1.67	1.67	1.61	.059
1030	1.45	1.42	1.39	1.51	1.64	1.73	1.54	.145
<hr/>								
1021-								
1030	2.07	2.09	2.02	2.08	2.12	2.23	2.11	.077
<hr/>								
1021-								
1030	1.84	1.82	1.80	1.89	1.98	2.07	1.91	.113

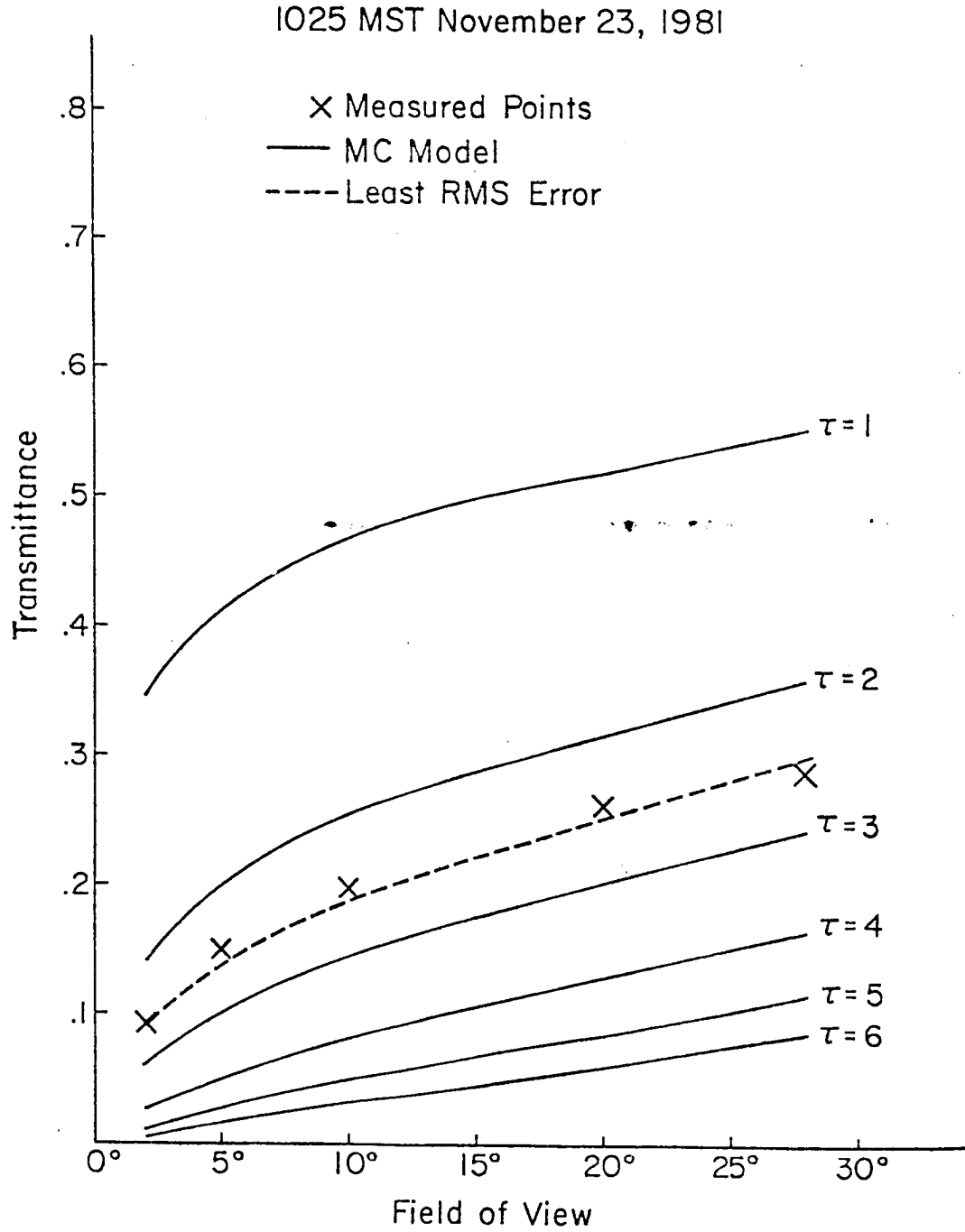


Figure 14a. Transmittance versus field of view for 1025 MST November 23, 1981.

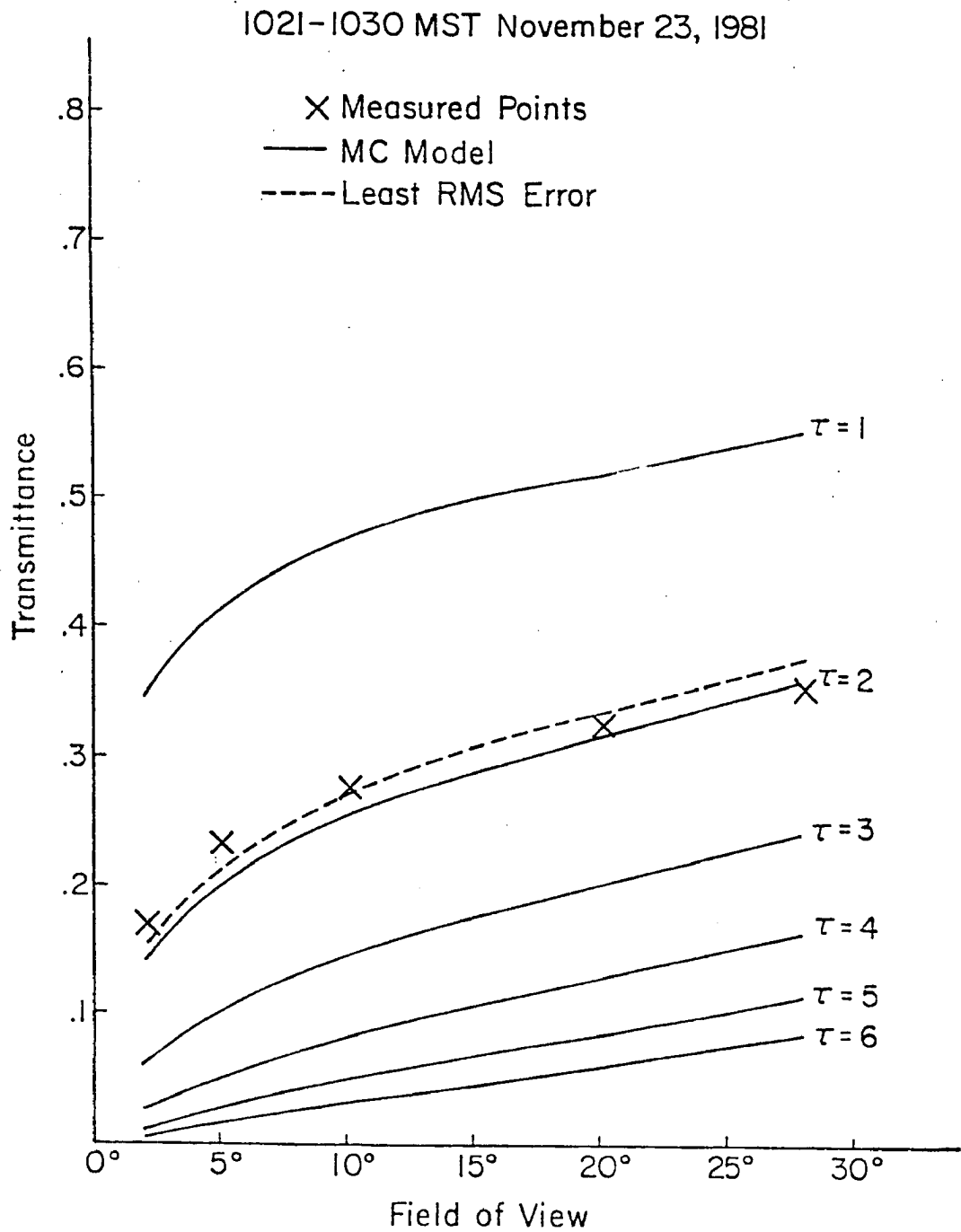


Figure 14b. Ten minute average values of transmittance versus field of view for the period 1021-1030 MST November 23, 1981.

Equation 19 produces an optical depth of 2.45 which is close to the average FOV value of 2.51. For the ten minute period, the equation gives 1.84 as the optical depth compared to 1.91 for the average. Again, the calculated values for both the instantaneous and average cases accurately represent the plotted points in Figures 14a and 14b. The smallest RMS errors are produced by model optical depths of 2.52 and 1.91 respectively. The model curves representing these optical depths are shown by the dashed lines in the figures.

As might be expected after examining the photograph of the cloud field, the total optical depths calculated during this ten minute period show considerable variability. Values of  $\tau$  range from .57 to 3.57 during the period owing to the broken nature of the cloud field. Surprisingly, however, the values of standard deviation are no larger than those determined from the previous cases which appeared to have a more uniform cloud fields. The range of standard deviations is somewhat larger than in the earlier cases, with values ranging from .037 to .280. This does give some indication of the broken nature of the cloud field. The pattern of the energy distribution to the five fields of view is consistent with earlier results. This is especially true of the ten minute average values of transmittance in Figure 14b.

### 5.23 Low Level Clouds

Three low cloud cases were examined. Two of these considered stratus type clouds and the third dealt with cumulus clouds.

January 12, 1982            1016-1025 MST

The cloud field present at this time consisted of thin stratus typically found along the Front Range during the breakup of upslope conditions. Again, no photographs were taken on this day.

The plot of transmittance versus field of view for 1020 MST is shown in Figure 15a. The data points in this figure would suggest an optical depth of approximately 3. The data points for the period 1016-1025 MST are shown in Figure 15b. These values of transmittance predict a lower optical depth probably near 2.75. The agreement between the model curves and the experimental values is somewhat worse than in the previous cases.

The calculated optical depths for 1016 to 1025 MST on January 12 are shown in Table 17. At 1020 MST, Equation 19 provides an optical depth of 2.83. This value is slightly lower than the value of 3.00 obtained from the five field of view. The difference between the methods is slightly greater for the ten minute period. Equation 19 produces a value of 2.46 compared to a value of 2.70 from the averaging method. Comparing these values with the data points in Figures 15a and 15b, it again appears that the average FOV optical depth is more accurate. The smallest RMS error curves in the two figures correspond to model optical depths of 3.05 for the one minute period and 2.74 for the ten minute period. These values also agree more closely with the average FOV optical depths.

The values of  $\tau$  in Table 17 range from 2.06 to 3.56 indicating that the cloud field was not uniform in thickness. This is not surprising when considering the type of stratus clouds which were present at this time. The standard deviations for this cloud case are more variable than those observed in the previous cloud cases. Values range from .074 at 1022 MST to .347 at 1016 MST indicating that the cloud field was very nonuniform. The data points in Figures 15a and 15b also show the nonuniformity of the cloud field. Both curves show

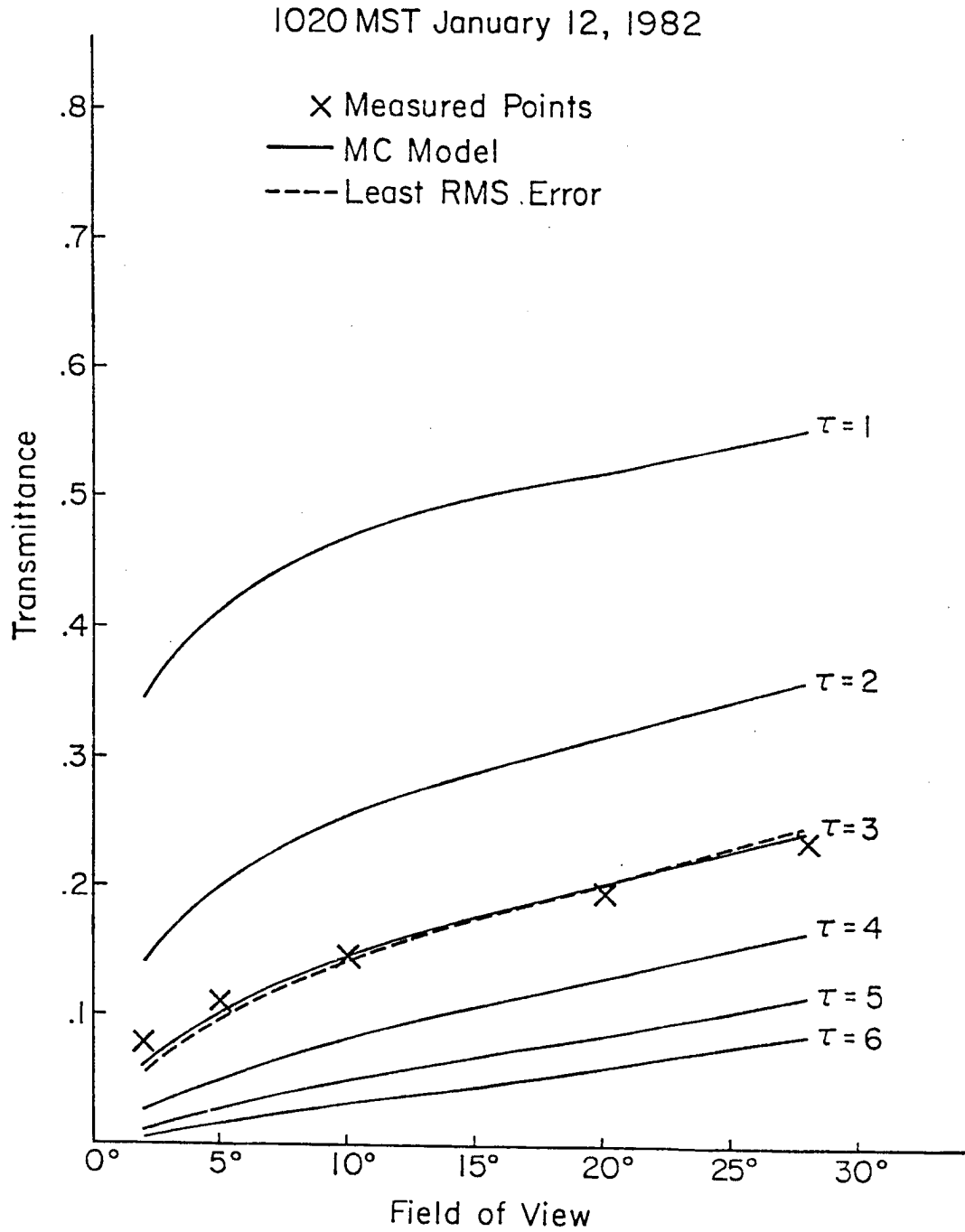


Figure 15a. Transmittance versus field of view for 1020 MST January 12, 1982.

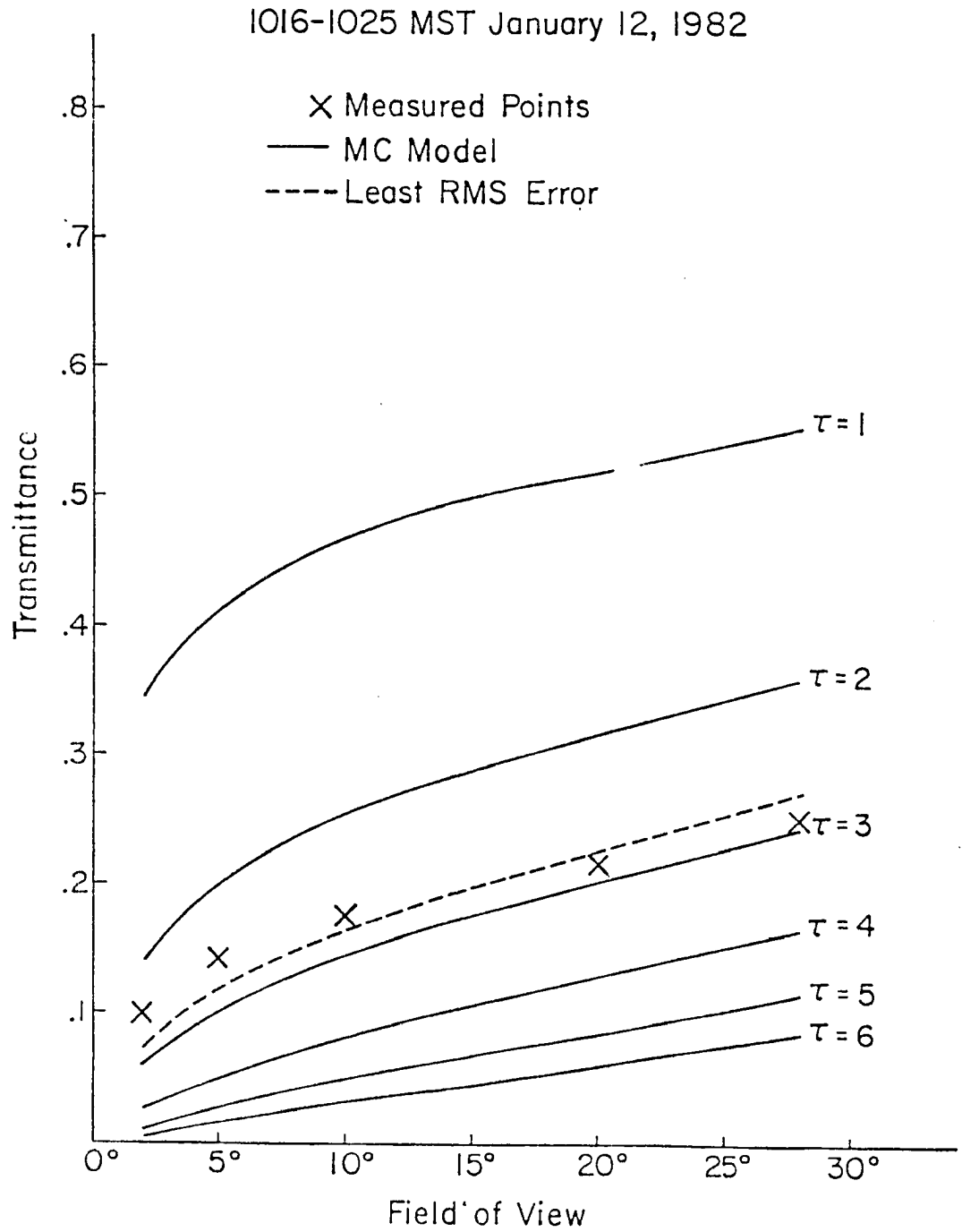


Figure 15b. Ten minute average values of transmittance versus field of view for the period 1016-1025 MST January 12, 1982.

less energy reaching the wider fields of view than expected which is consistent with the results from previous cases.

Table 17. Calculated optical depths for the period 1016-1025 MST  
January 12, 1982.

TIME	$\tau_{EQ}$	$\tau_2$	$\tau_5$	$\tau_{10}$	$\tau_{20}$	$\tau_{28}$	$\tau_{AVE}$	$\sigma$
1016	2.30	2.24	2.37	2.61	2.89	3.07	2.64	.347
1017	2.38	2.32	2.46	2.68	2.94	3.12	2.70	.330
1018	2.29	2.21	2.30	2.48	2.66	2.78	2.49	.299
1019	1.90	1.84	1.87	2.03	2.23	2.33	2.06	.216
1020	2.83	2.73	2.89	3.02	3.14	3.21	3.00	.193
1021	2.23	2.17	2.21	2.34	2.52	2.58	2.36	.182
1022	3.25	3.32	3.52	3.47	3.46	3.44	3.44	.074
1023	3.22	3.20	3.38	3.47	3.62	3.68	3.47	.192
1024	3.27	3.20	3.39	3.56	3.78	3.87	3.56	.275
1025	1.91	1.90	1.89	2.02	2.24	2.31	2.07	.194
1016-								
1025	2.56	2.51	2.63	2.77	2.95	3.04	2.78	.219
1016-								
1025	2.46	2.40	2.52	2.68	2.89	2.99	2.70	.246

January 12, 1982            1326-1335 MST

The second low cloud case considers a stratus cloud which is less dense than the previous case and more uniform in nature. There is also much less total cloud cover than was observed for the earlier January 12th case.

AT 1330 MST, the experimental transmittance values in Figure 15c suggest an optical depth between 1.50 and 2.0. In comparison, the ten minute average values of transmittance plotted in Figure 15d provide an optical depth closer to 1.50. For both the instantaneous and ten minute average cases, the data points show the best agreement so far with the model curves.

The calculated values of optical depth are shown in Table 18. The two methods of computation provide values of  $\tau$  of 1.91 and 1.75 for 1330 MST and 1.70 and 1.52 as the average optical depth for 1326-1335 MST. These results are similar to the results from the first two high cloud cases in that Equation 19 again predicts a higher optical depth than the averaging method. The average of the FOV optical depths again seems to more accurately represent the  $\tau$  values predicted by the data points in Figures 15c and 15d. The optical depths corresponding to the least RMS error between experimental and model transmittance values were found to be 1.76 and 1.52 for the one and ten minute cases. The curves of transmittance versus field of view for these optical depths fit the data points very well as shown in the two figures.

As with many of the previous cases, the total optical depth of the cloud changes significantly during the ten minute period. Average  $\tau$  values range from .16 to 2.81 with the small optical depth's occurring

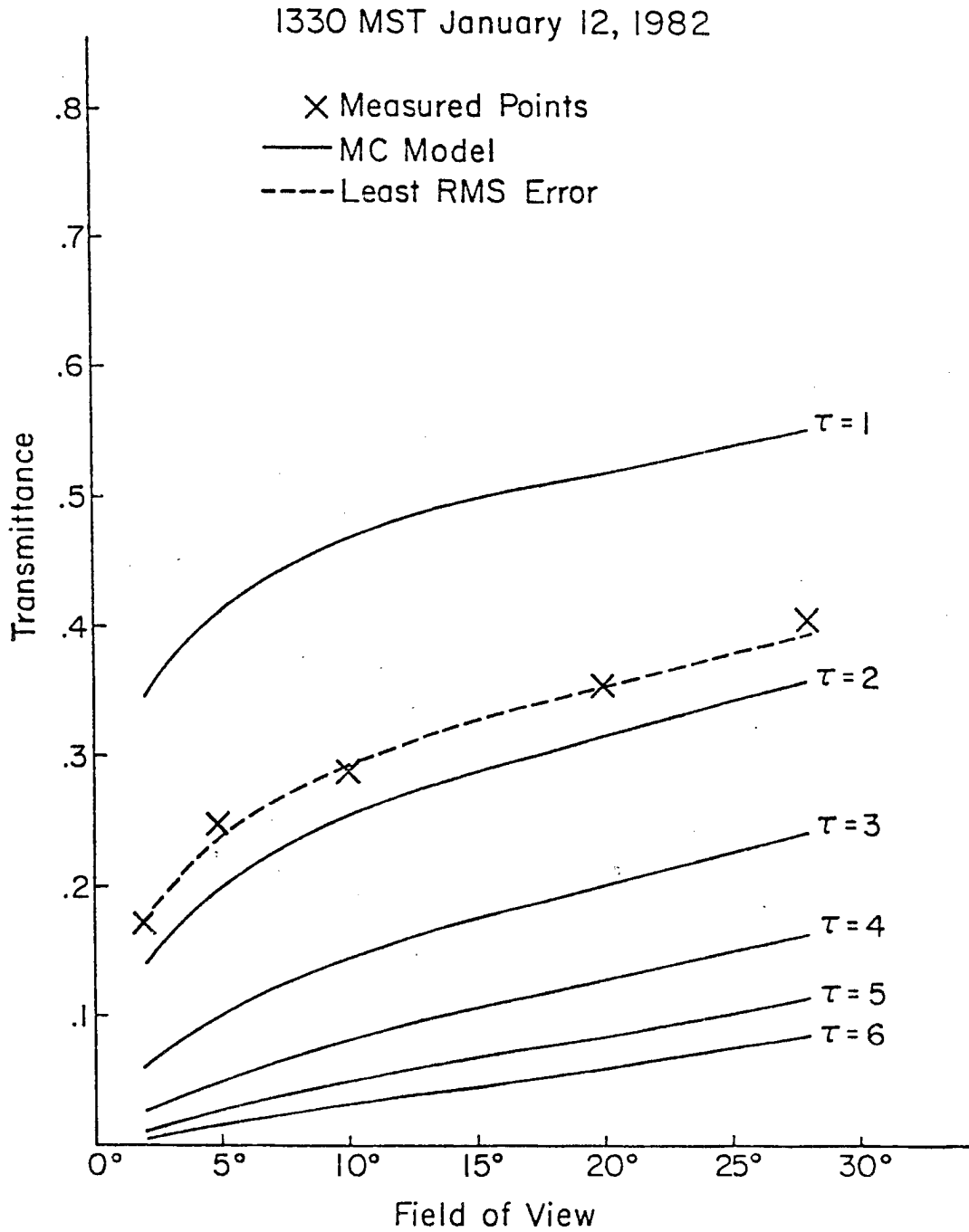


Figure 15c. Transmittance versus field of view for 1330 MST January 12, 1982.

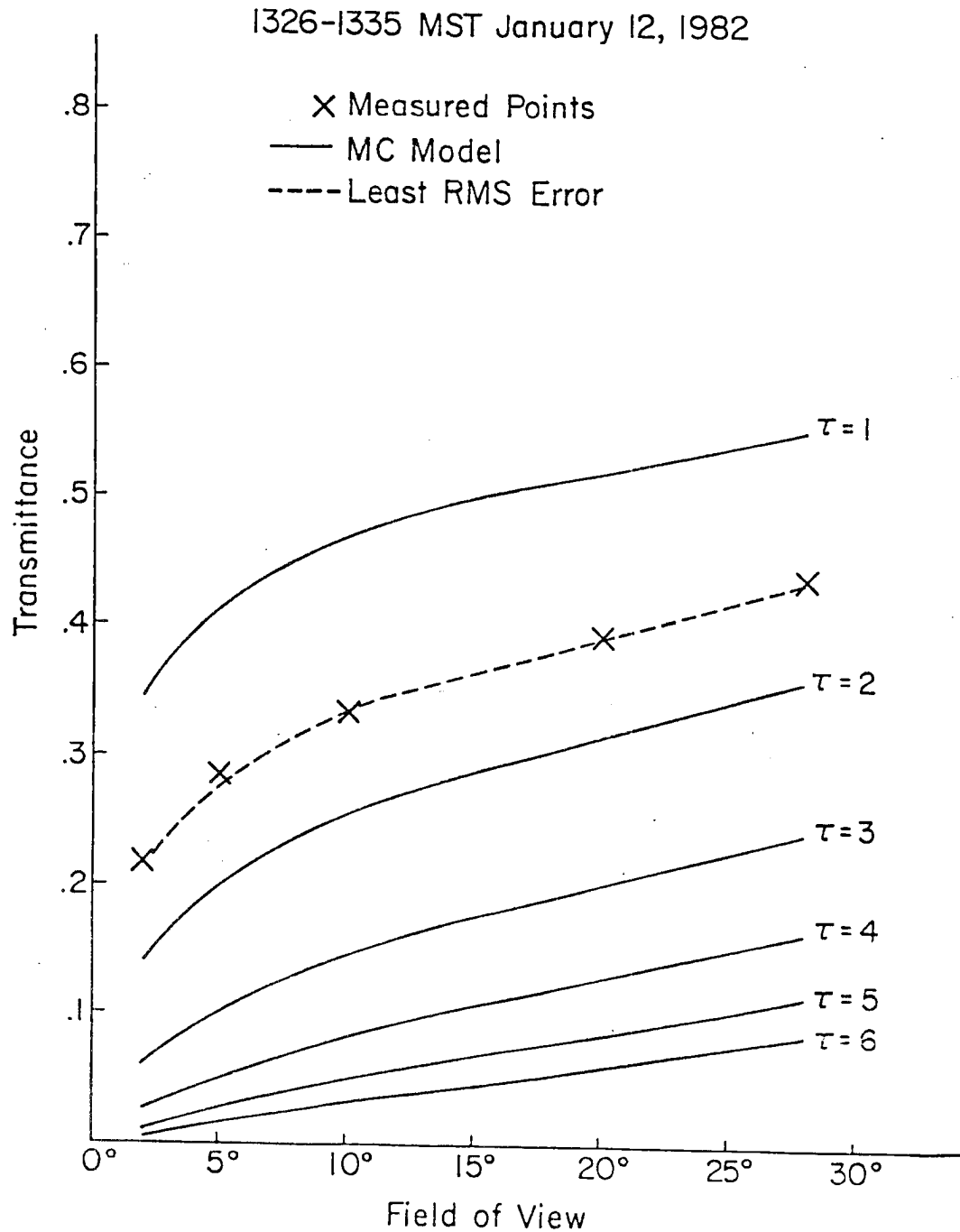


Figure 15d. Ten minute average values of transmittance versus field of view for the period 1326-1335 MST January 12, 1982.

at the end of the ten minute period indicating that the clouds had virtually disappeared at this time. During the first five minutes,  $\sigma$  values were very small except for the 1327 MST case. This would suggest that the cloud field was very uniform at least for a short period of time. Even more interesting is the small standard deviation obtained for the ten minute average  $\tau$  especially considering the wide range of values found during the period. The  $\tau$  values obtained during the last three minutes of the period are quite variable as indicated by the large standard deviation. This is probably due to the fact that the sun was either in or near the edge of the cloud. The pattern where less energy than expected reaches the wide fields of view found in most of the case studies continues to some degree in this case. However, for most of the ten minute period, the  $28^\circ$  FOV predicts a lower optical depth than the average value instead of higher.

Table 18. Calculated optical depth for the period 1326-1335 MST  
January 12, 1982.

TIME	$\tau_{EQ}$	$\tau_2$	$\tau_5$	$\tau_{10}$	$\tau_{20}$	$\tau_{28}$	$\tau_{AVE}$	$\sigma$
1326	2.19	2.09	2.10	2.13	2.12	2.09	2.11	.019
1327	2.69	2.69	2.64	2.56	2.44	2.37	2.54	.134
1328	1.87	1.76	1.73	1.76	1.74	1.68	1.73	.033
1329	1.69	1.57	1.51	1.55	1.53	1.47	1.53	.039
1330	1.91	1.77	1.74	1.79	1.77	1.70	1.75	.035
1331	2.46	2.45	2.42	2.37	2.28	2.24	2.35	.090
1332	2.82	2.91	2.86	2.79	2.74	2.74	2.81	.075
1333	2.09	1.89	1.93	2.24	2.49	2.69	2.25	.348
1334	.64	.42	.20	.16	.01	.001	.16	.171
1335	.77	.55	.37	.37	.27	.09	.33	.168
<hr/>								
1326-								
1335	1.91	1.81	1.75	1.77	1.74	1.71	1.76	.037
<hr/>								
1326-								
1335	1.70	1.53	1.49	1.55	1.55	1.49	1.52	.030

April 15, 1982

1426-1435 MST

The final low cloud case considers a dense cumulus field which contains several holes. The cloud cover at 1425 MST is shown in Figure 16. This cumulus cloud was chosen because it shows how the procedure outlined above performs when the sun is located in an optically thin medium surrounded by clouds which are much more dense.

The transmittance versus field of view plot for 1430 MST is shown in Figure 15e. As the X's in the figure indicate, the agreement between model and experiment is very poor. Similar results are

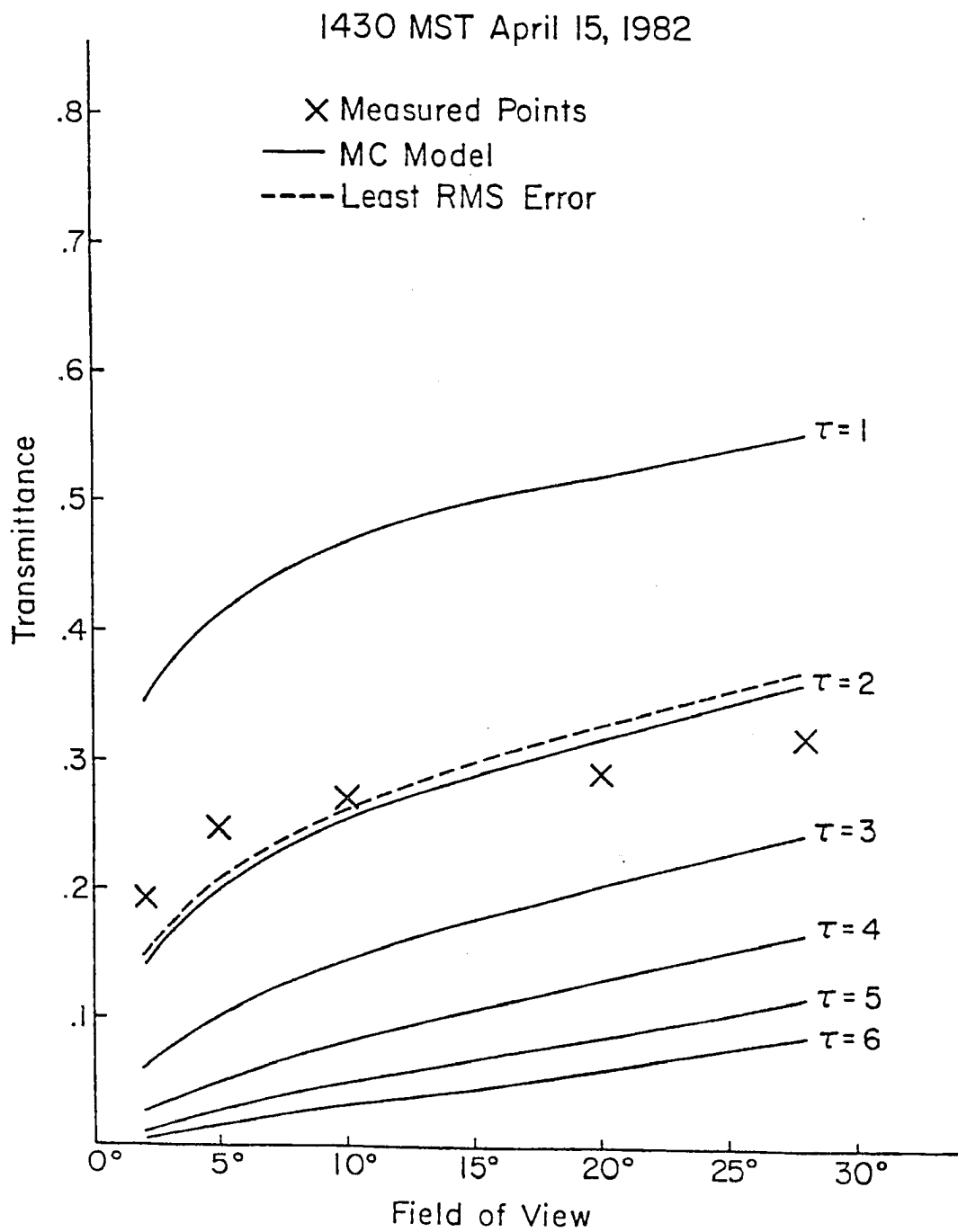


Figure 15e. Transmittance versus field of view for 1430 MST April 15, 1982.

obtained with the ten minute average transmittance values shown in Figure 15f. Although the points in this figure indicate that the optical depth is larger than the one minute case, the agreement with the model is still very poor.

The calculated values of optical depth for the April 15th case are shown in Table 19. At 1430 MST, Equation 19 produces an optical depth of 1.81 which is less than the value of 1.97 obtained from the average of the five field of view optical depths. The average optical depth for the ten minute period was determined to be 2.69 using the single equation and 3.12 using the average from the five instruments. The model transmittances producing the smallest RMS errors with the actual data points corresponded to optical depths of 1.95 for the instantaneous case and 3.25 for the ten minute average. Again, the averaging method appears to more accurately represent the plotted points in the two figures.

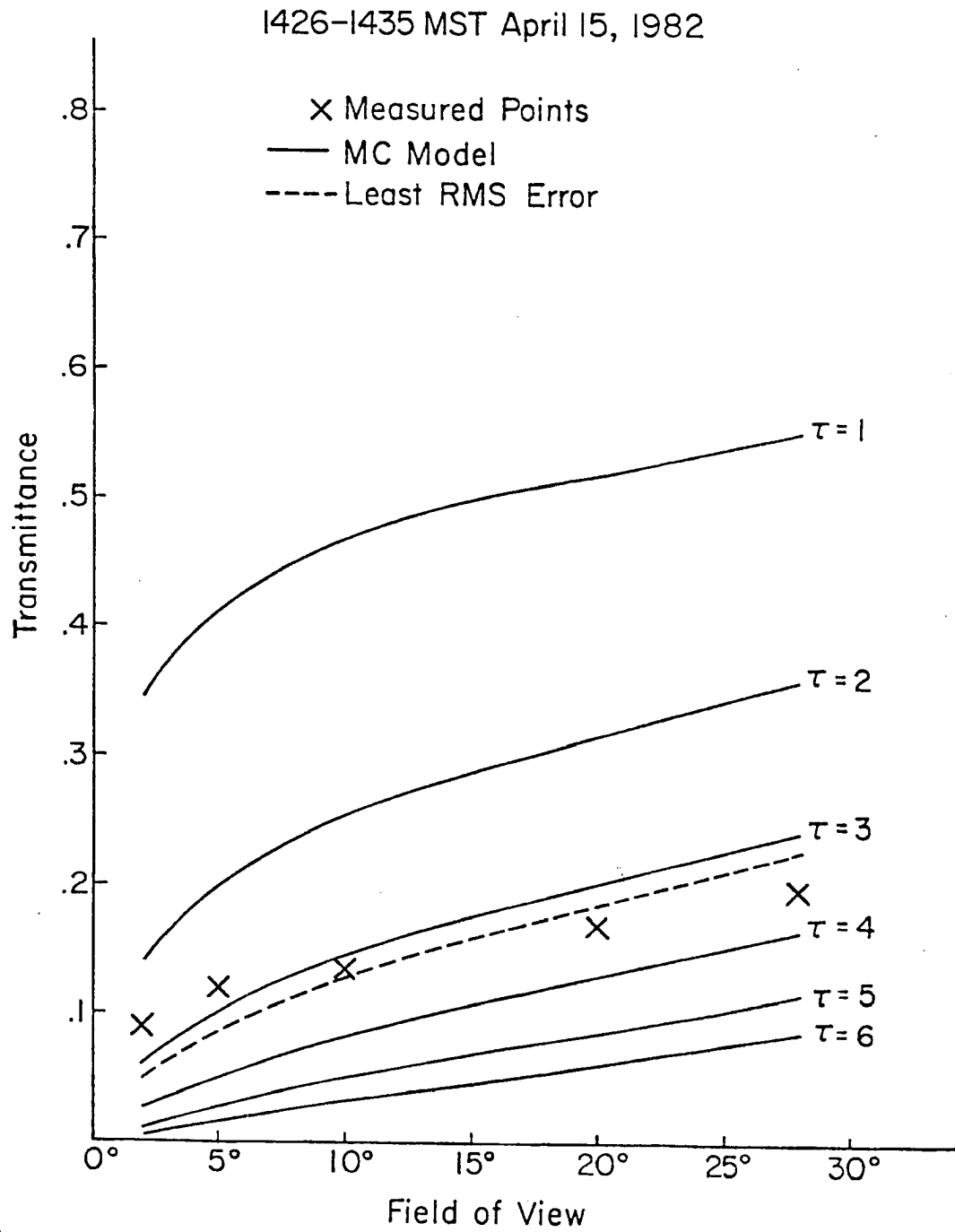


Figure 15f. Ten minute average values of transmittance versus field of view for the period 1426-1435 MST April 15, 1982.



Figure 16. Photograph of cloud cover at 1425 MST April 15, 1982.

Table 19. Calculated optical depths for the period 1426-1435 MST  
April 15, 1982.

TIME	$\tau_{EQ}$	$\tau_2$	$\tau_5$	$\tau_{10}$	$\tau_{20}$	$\tau_{28}$	$\tau_{AVE}$	$\sigma$
1426	4.20	4.09	4.50	4.80	5.11	5.35	4.77	.497
1427	4.70	4.51	4.98	5.53	6.11	6.54	5.53	.821
1428	5.36	5.09	5.54	5.84	6.13	6.20	5.76	.457
1429	8.22	7.91	8.39	8.32	7.67	7.71	8.00	.337
1430	1.81	1.64	1.70	1.90	2.22	2.38	1.97	.323
1431	1.96	1.92	1.97	2.17	2.48	2.60	2.23	.303
1432	4.12	4.87	5.27	4.46	3.82	3.60	4.40	.700
1433	1.93	1.86	2.01	2.26	2.59	2.76	2.30	.379
1434	1.54	1.41	1.42	1.56	1.72	1.73	1.57	.155
1435	2.77	2.59	2.86	3.24	3.67	3.91	3.25	.548
1436-								
1435	3.66	3.59	3.86	4.01	4.15	4.28	3.98	.268
1426-								
1435	2.69	2.55	2.80	3.11	3.48	3.67	3.12	.464

The range of optical depths during this ten minute period is the largest found in any of the case studies. Values of  $\tau$  range from 1.57 at 1434 MST to 8.00 at 1429 MST. The standard deviations determined for this case are also quite large. The maximum  $\sigma$  occurred at 1427 MST and had a value of .821. At 1427 MST, the optical depths calculated for the five fields of view range from 4.51 to 6.54. The large variations in  $\tau$  both from minute to minute and among the five

fields of view are not surprising considering the nature of the cloud field. When the sun is in a hole in the cloud, the small fields of view show a lower optical depth than the wider fields of view. The energy which would normally reach the wider fields is either scattered at large angles or absorbed by the dense cloud around the sun. This type of cloud field can also produce the opposite effect. At 1432 MST, the wide fields of view actually produce lower optical depths than the small fields. There are two possible causes for this. One possibility is that reflected energy from the side of the dense cloud layer reaches the wide fields of view causing a lower optical depth to be predicted. A second possibility would find an optically dense cloud "over" the sun with much thinner clouds in the area around the sun. More scattered energy could then reach the wide fields of view and lead to a lower optical depth. The experimental curves in Figures 15e and 15f show the first situation very well.

### 5.3 Discussion

As mentioned several times during the case study analysis, the wide fields of view consistently indicated larger optical depths than the small fields of view. The only explanation presented to this point was that the cloud fields examined were nonhomogeneous thus causing the scattering of energy to be different than predicted by the Monte Carlo model for a uniform cloud. In some of the case studies, the nature of the cloud cover appeared to be the major factor affecting the transmittance at each FOV. On October 26th and April 15th, the sun was in or near a region of dense clouds which prevented energy from reaching the wide fields of view.

Other factors may also play a role in causing the discrepancy between model and experiment. First, the model was run using a Best droplet distribution for spherical water drops whereas most of the case study situations contained ice clouds. It is possible that the scattering from ice crystals is different than for water droplets. Jacobowitz (1971) investigated the transfer of solar radiation through hexagonal ice crystals. He compared the intensity pattern from randomly oriented prisms with that from equivalent spheres of radii 25  $\mu\text{m}$ . Figure 17 is Jacobowitz's plot of intensity versus scattering angle for both crystals and spheres. The curve for the crystals shows less intensity than for the spheres at scattering angles between  $5^\circ$  and  $20^\circ$ . The curves are the same below  $4^\circ$  because the diffraction was assumed to be the same for both the spheres and the ice crystals. The result for the crystals indicates that this may be a contributing factor to the scattering patterns shown in the case studies.

If one is dealing only with water clouds, then a second factor which may effect the scattering of the incoming radiation is drop size. For the Best droplet distribution, the mean droplet radius is 10  $\mu\text{m}$ . Different droplet sizes may produce different scattering results than those presented in this paper. Kattawar and Plass (1967) investigated this possibility. They calculated the single scattering phase function for four droplet distributions which were called Haze Continental, Haze Maritime, Cumulus, and Nimbostratus. Figure 18 shows the scattering functions for the four droplet distributions as well as for isotropic and Rayleigh scattering. The droplet radii for the four distributions range from .03 to greater than 12  $\mu\text{m}$ . The only major differences in the curves occur at scattering angles less than  $4^\circ$

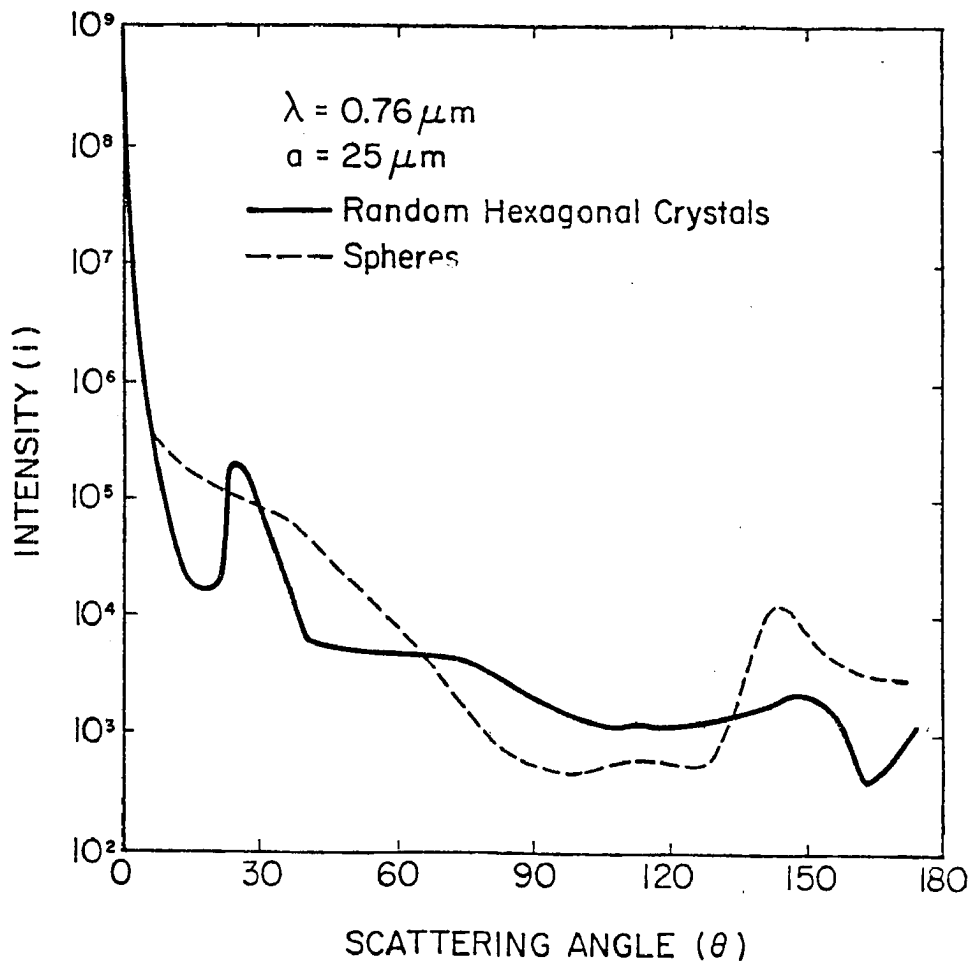


Figure 17. Total intensity,  $i$ , for randomly oriented hexagonal prisms compared with that for spheres versus scattering angle  $\theta$ . (Reproduced from Figure 3 of Jacobowitz (1971)).

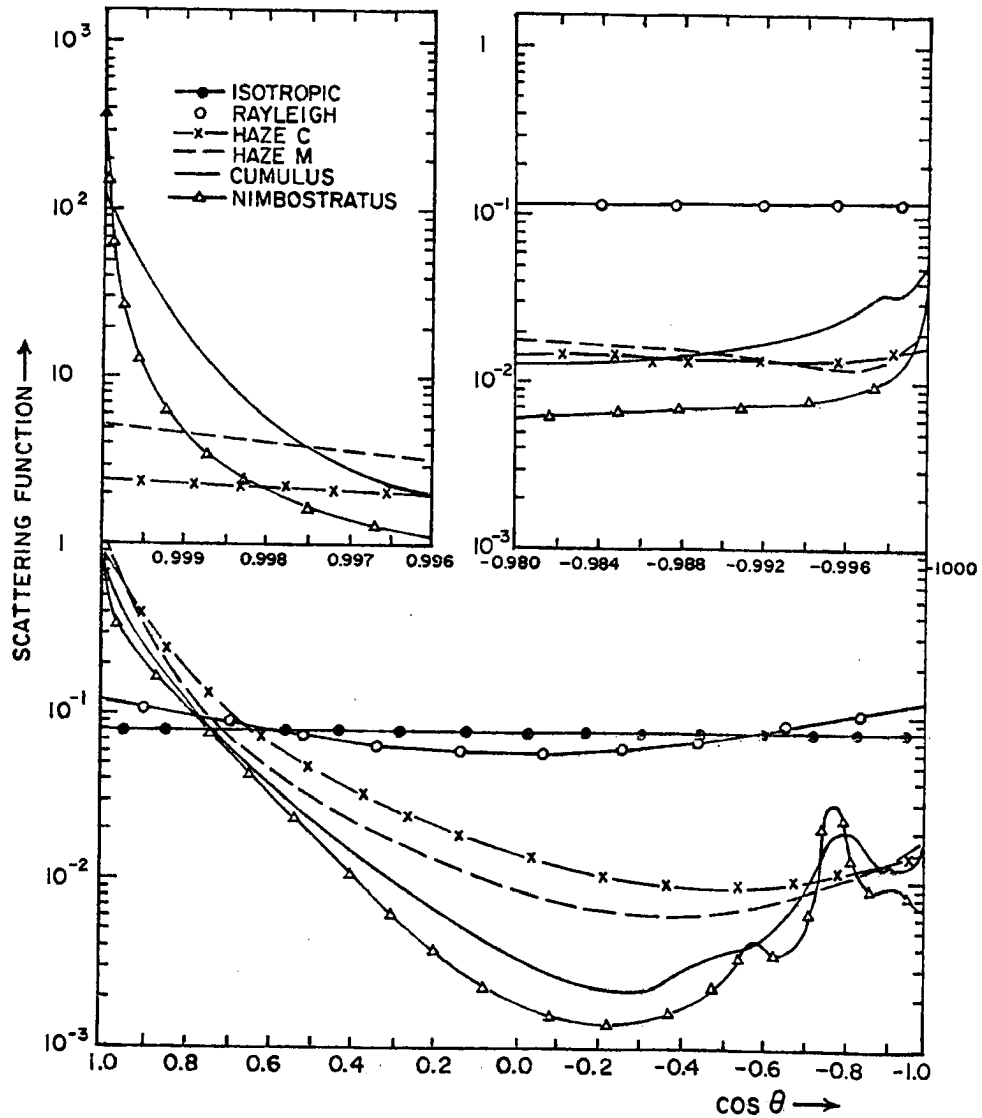


Figure 18. The angular scattering function for Mie scattering as a function of the cosine of the scattering angle  $\theta$  for six particle size distributions. The inset in the upper left shows the curves near  $\mu = 1$  and in the upper right near  $\mu = -1$ . (Reproduced from Figure 1 of Kattawar and Plass (1967)).

and reflect the strength of the forward scattering peak. This would indicate that droplet size may have some effect on the results in the case studies but the probable effect would be minimal especially at the wider fields of view. Since little data was collected with water clouds, a comparison with the results from the ice clouds would be inconclusive.

In examining the agreement between model and experiment, two methods of calculating the cloud optical depth were used. Consistently, the method whereby an average of the optical depths calculated at each field of view more accurately represented the optical depth predicted in the plots of transmittance versus FOV. This seems to be due to the fact that Equation 19 is more sensitive than the averaging method to irregularities in the transmittance values. As a comparison of the sensitivity of the two methods, the five model transmittances for a  $\tau$  of 3 were varied in the following manner. First, the  $2^\circ$  and  $5^\circ$  values of T were reduced by 20 and 10 percent respectively, the  $20^\circ$  and  $28^\circ$  values of T were increased by 10 and 20 percent respectively and the  $10^\circ$  T value was left unchanged. In the second case, the  $2^\circ$  and  $5^\circ$  values were increased and the  $20^\circ$  and  $28^\circ$  values were decreased. New optical depths were then calculated using each method. In both situations, the averaging method showed much less of a change in  $\tau$  from the original value of 3 and also produced an optical depth which was close to the optical depth corresponding to the smallest RMS error between experimental and model transmittances. A summary of these calculations is shown in Table 20.

Table 20. Results of the sensitivity test on the two methods of calculating cloud optical depth.

Transmittance	% Change From $\tau = 3$ values	$\tau_{EQ}$	$\tau_{AVE}$	$\tau_{RMS}$
.0483	-20			
.0915	-10			
.1437	0	3.36	2.98	2.90
.2203	10			
.2908	20			
.0725	+20			
.1119	+10			
.1437	0	2.58	3.14	3.23
.1803	-10			
.1938	-20			

Also of note in the data tables are the two rows of ten minute average values of optical depth. The first row is the simple linear average of the ten optical depths calculated each minute. The second row shows the optical depth determined when the ten minute average values of transmittance are used in the two methods of calculation. In some of the case studies the agreement between the two sets of averages was very poor and in all cases, the second set of values was smaller than the first. The magnitude of the difference between the sets of ten minute averages seems to be somewhat dependent on the range of optical depths during the period. For example, on October 28th,  $\tau$  values ranged from .58 to .98 for a difference of .4. In this

case, there was almost no difference between the two sets of ten minute averages. In contrast, on April 15th, optical depth ranged from 1.57 to 8.00 for a difference of 6.43. The difference in ten minute average values for this case was as large as 1.06. The discrepancy is due to the fact that the relationship between transmittance and optical depth is not a linear one as shown in Figure 10.

Even though the case studies show that the photodiode radiometer can in most cases be effectively used to determine the optical depth of thin clouds, the ideas above suggest some of the improvements which can be made in the system.

1) The first and most obvious improvement to aid in judging the effectiveness of the method described in this paper to determine cloud optical depth is to collect more data with different cloud types. At present, data has been collected for only 15 days and most of the data were collected for high clouds. As mentioned, only one day was available with either cumulus or stratus clouds. It would be especially desirable to have more data available for water clouds.

2) Another possible way to improve the comparison between model and experiment would be to run the model using Legendre scattering coefficients for different droplet distributions or ice crystal shapes. The major deterrent to doing this are the large amounts of computer time which would be required to make the model runs. Also, the scattering coefficients are hard to obtain.

3) Model calculations of vapor and droplet absorption could be made with atmospheric soundings which contain more moisture than the midlatitude winter sounding which was used. This would be especially

desirable for comparison with data collected during the summer when the atmosphere contains more water vapor.

4) The final improvement concerns the hardware itself. At present the collimator tubes are not weatherproofed. This was done to avoid any effects a glass or plastic cover might have on the incident radiation. From experience, however, weatherproofing seems to be almost essential if continuous operation is desired.

## 6.0 CONCLUSION

A method has been described which examines the feasibility of using a photodiode radiometer to infer optical depth of thin clouds from solar intensity measurements. The photodiode radiometer measures incident radiation at angular fields of view of 2°, 5°, 10°, 20° and 28°. Using measurements from the photodiodes, a pyrliometer, and a pyranometer, values of normalized annular radiance and transmittance were calculated for various cloud fields. The observations were compared with similar calculations made using the results obtained from a Monte Carlo radiative transfer model. The model used a Best droplet distribution for horizontally infinite and homogeneous water clouds of optical depth 1 through 6 at spectral bandpasses of 0.3 to 0.8 and 0.8 to 2.8  $\mu\text{m}$ .

Normalized radiances and transmittances derived from the model and from observations were compared for high, middle, and low cloud cases using both graphical and mathematical methods. Only the comparison of optical depth determined from the transmittances was presented since the transmittances proved much more reliable in producing the expected  $\tau$  values. The graphical comparison was made using plots of transmittance versus field of view for both model and experimental results. A best fit model curve was determined for the data by calculating the minimum RMS error between model and experimental transmittances at optical depths close to the expected value. To verify the graphical prediction, an experimental cloud

optical depth was calculated by two methods. A single equation was derived which used the transmittance values from the five fields of view to produce a cloud optical depth. The second method involved calculating a  $\tau$  value for each field of view and averaging the five values. For each cloud case, instantaneous and average values were calculated over a ten minute time period.

Four high cloud cases having varying optical thickness and uniformity were examined. The best agreement between model and experiment occurred for a thin cirrus cloud field. Average FOV  $\tau$  values ranged from .58 to .98 with the maximum standard deviation being only .118. These average values agreed very well with the graphically predicted values. The single equation values were larger than the average  $\tau$ 's and showed less agreement with the plotted points. The largest discrepancy between model and experiment occurred with the sun behind a cirrocumulus layer and in the vicinity of a dense altocumulus layer. The cloud optical depths for this period ranged from 1.58 to 3.45 with a maximum standard deviation of .262. Again the average  $\tau$  value provided a better representation of the cloud optical depth than the single equation.

One mid-level cloud case consisting of broken altocumulus was examined.  $\tau$  ranged from .57 to 3.57 with the largest standard deviation being .280. The results for this case are similar to the high cloud cases with the exception being the greater range of  $\tau$  and  $\sigma$  values during the ten minute period.

The three low cloud cases examined consisted of two stratus and one cumulus cloud field. Observations from the second stratus case showed the best agreement between model and experiment of all the

cases examined. The  $\tau$  values ranged from .16 to 2.81 with the largest standard deviation being .348. This large standard deviation is somewhat misleading in that the other values during this ten minute period were all less than .171 and four of the  $\sigma$ 's were less than .04. The large values occurred when the sun was near the edge of the cloud. In contrast, the cumulus cloud field produced the worst agreement with the model. Optical depths ranged from 1.57 to 8.00 with a maximum standard deviation of .821. The large discrepancy between the model and experiment is due to the fact that holes exist in the cumulus cloud.

In all of the case studies, the average FOV optical depth was more representative of the plotted data points than the single equation value. It appears that this is due to the sensitivity of the single equation to differences between expected and actual transmittances for a given optical depth.

The results of the case studies showed a rather consistent pattern where the wide fields of view produced a larger optical depth than the small fields of view. Several possible explanations were proposed. Nonhomogeneities in the cloud field may cause less energy to reach the wide fields of view than would normally be the case. This definitely appears to be true for the high cloud case where the dense altocumulus was present as well as for the cumulus cloud field. A second possible explanation is the fact that the Monte Carlo model was run using a Best droplet distribution for spherical water drops while the case studies dealt mainly with ice clouds. Jacobowitz (1971) indicates that the scattering from hexagonal ice crystals is somewhat different than for spherical drops. Finally, for cases where

water clouds were present, drop size may also be important. Kattawar and Plass (1967) indicate that the scattering function does vary at small scattering angles for different drop size distributions.

On the basis of the analysis of the case studies presented above, the photodiode radiometer shows real promise as an effective tool for measuring optical depth of thin clouds. Results derived from radiometer measurements showed exceptional agreement with theory for a variety of cloud types and cloud cover situations. The only exception occurred when a rather nonuniform cumulus cloud field was present. It is likely that even better results may be achieved if the improvements discussed earlier in this paper are implemented.

The photodiode radiometer also shows potential for other uses. Since the  $2^\circ$  field of view instrument measures almost exclusively the direct solar beam, it could conceivably be used as a tool for determining sunshine duration. Other valuable information about the nature of the cloud cover could be gained by examining the standard deviation about the average of the five field of view optical depths. In general, both clear sky and uniform cloud fields would produce small  $\sigma$ 's while heterogeneous cloud fields would produce large values. Finally, even though results from the heterogeneous cloud cases do not agree with theory, the photodiode radiometer may actually provide advantages in determining an optical depth for these types of clouds.

## REFERENCES

- Bowling, Sue Ann, 1972: Comments on "Cirrus Clouds and Climate." J. Atmos. Sci., 29, 1003.
- Cess, R. D., 1976: Climate Change: An Appraisal of Atmospheric Feedback Mechanisms Employing Zonal Climatology J. Atmos. Sci. 33, 1831-1843.
- Cess, R. D. and V. Ramanathan, 1978: Averaging of Infrared Cloud Opacities for Climate Modeling. J. of Atmos. Sci., 35, 919-922.
- Coulson, K. L., 1975: Solar and Terrestrial Radiation. Academic Press, Inc., New York, 320 pp.
- Cox, S. K., 1971: Cirrus Clouds and Climate. J. Atmos. Sci. 28, 1513-1515.
- Davis, J. M., S. K. Cox, and T. B. McKee, 1979: Total Shortwave Radiative Characteristics of Absorbing Finite Clouds. J. Atmos. Sci., 36, 508-518.
- Ellis, J. S., 1978: Cloudiness, The Planetary Radiation, Budget and Climate. Ph.D. Dissertation, Colorado State University, 129 pp.
- Jacobowitz, H., 1971: A Method for Computing the Transfer of Solar Radiation Through Clouds of Hexagonal Ice Crystals. J. Quant. Spectrosc. and Radiat. Transfer, 11, 691-695.
- Kasten, F. and E. Raschke, 1974: Reflection and Transmission Terminology by Analogy with Scattering. Appl. Optics, 13, 460-464.
- Kattawar, G. W. and G. N. Plass, 1967: Influence of Particle Size Distribution on Reflected and Transmitted Light from Clouds. AF19(628)-5039-- Southwest Center for Advanced Studies, Dallas, Texas.
- Liou, K. N. and T. Sasamori, 1975: On the Transfer of Solar Radiation in Aerosol Atmospheres. J. Atmos. Sci., 32, 2166-2177.
- Manabe, S. and R. Strickler, 1964: Thermal Equilibrium of the Atmosphere with a Convective Adjustment. J. Atmos. Sci., 21, 361-385.

- McClatchey, R. A., R. W. Fenn, J. E. A. Selby, F. E. Volz and J. S. Garing, 1971: Optical properties of the Atmosphere. Environmental Research Paper No. 354, AFCRL, 85 pp. [NTIS AD 726 116].
- McKee, T. B. and S. K. Cox, 1974: Scattering of Visible Radiation by Finite Clouds. J. Atmos. Sci., 31, 1885-1892.
- Noble, B., 1969: Applied Linear Algebra. Prentice Hall, Inc., Edgewood Cliffs, N.J., 523 pp.
- Ohring, G. and P. Clapp, 1980: The Effect of Changes in Cloud Amount on the Net Radiation at the Top of the Atmosphere. J. Atmos. Sci., 37, 447-454.
- Ohring, G. and S. Adler, 1978: Some Experiments with a Zonally Averaged Climate Model. J. Atmos. Sci., 35, 186-205.
- Stephens, G. L., 1978: Radiation Profiles in Extended Water Clouds. II: Parameterization Schemes. J. Atmos. Sci., 35, 2123-2132.
- Thompson, T. M. and S. K. Cox, 1982: Subtropical Climatology of Direct Beam Solar Radiation. J. of Appl. Meteor., 21, 334-338.
- Twomey, S., 1976: Computations of the Absorption of Solar Radiation by Clouds. J. Atmos. Sci., 33, 1087-1091.
- Welch, R. M., S. K. Cox, and T. M. Davis, 1980: Solar Radiation and Clouds. American Meteorological Society, 96 pp.
- Zdunkowski, W. G., B. C. Nielson, and G. Korb, 1967: Prediction and Maintenance of Radiation Fog. Technical Report ECOM-0049-F, USAEC, Fort Monmouth, N. J.

BIBLIOGRAPHIC DATA SHEET		1. Report No.	2.	3. Recipient's Accession No.	
4. Title and Subtitle				5. Report Date	
The Determination of Cloud Optical Depth from Multiple Fields of View Pyrheliometric Measurements				December, 1982	
6.				7. Author(s)	
				Robert Raschke and Stephen K. Cox	
9. Performing Organization Name and Address				8. Performing Organization Rept. No.	
Department of Atmospheric Science Colorado State University Fort Collins, CO 80523				CSU-ATS-	
10. Project/Task/Work Unit No.				11. Contract/Grant No.	
				ATM-8010691	
12. Sponsoring Organization Name and Address				13. Type of Report & Period Covered	
National Science Foundation					
14.					
15. Supplementary Notes					
16. Abstracts					
<p>The feasibility of using a photodiode radiometer to infer optical depth of thin clouds from solar intensity measurements was examined. Data were collected from a photodiode radiometer which measures incident radiation at angular fields of view of 2°, 5°, 10°, 20°, and 28°. In combination with a pyrheliometer and pyranometer, values of normalized annular radiance and transmittance were calculated. Similar calculations were made with the results of a Monte Carlo radiative transfer model. The Monte Carlo results were for cloud optical depths of 1 through 6 over a spectral bandpass of 0.3 to 2.8 μm.</p> <p>Eight case studies involving various types of high, middle, and low clouds were examined. Experimental values of cloud optical depth were determined by three methods. Plots of transmittance versus field of view were compared with the model curves for the six optical depths which were run in order to obtain a value of cloud optical depth. Optical depth was then determined mathematically from a single equation which used the five field of view transmittances and as the average of the five optical depths calculated at each field of view. Analysis of the case study results indicates that the photodiode radiometer can be used effectively to determine the optical depth of thin clouds.</p>					
17. Key Words and Document Analysis. 17a. Descriptors					
17b. Identifiers/Open-Ended Terms					
17c. COSATI Field/Group					
18. Availability Statement			19. Security Class (This Report)		21. No. of Pages
			UNCLASSIFIED		94
			20. Security Class (This Page)		22. Price
			UNCLASSIFIED		